A319

UCRL- JC-106039
PREPRINT

ANALYSIS OF OIL SHALE AND PETROLEUM SOURCE ROCK PYROLYSIS BY TRIPLE QUADRUPOLE MASS SPECTROMETRY: COMPARISONS OF GAS EVOLUTION AT THE HEATING RATE OF 10°C/MIN

JOHN G. REYNOLDS
RICHARD W. CRAWFORD
ALAN K. BURNHAM

This Paper was Prepared for Submittal to
Fuel and Energy

October 5, 1990

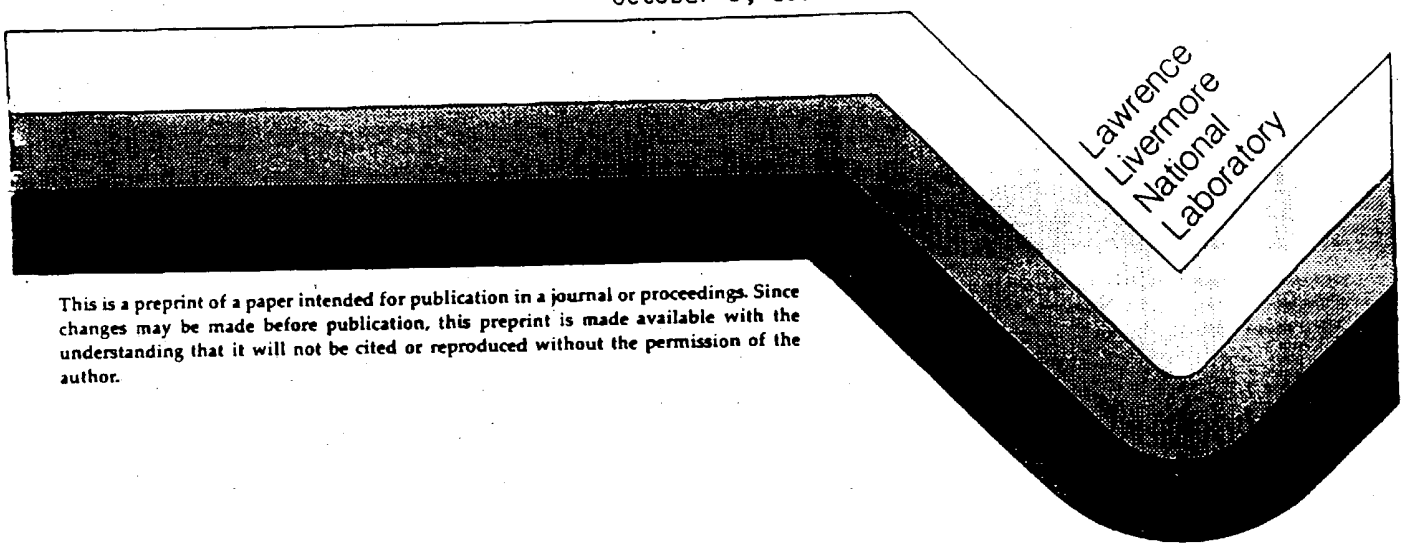

Revised 10/01/90
Version 21

Analysis of Oil Shale and Petroleum Source Rock Pyrolysis by Triple Quadrupole Mass Spectrometry: Comparisons of Gas Evolution at the Heating Rate of 10 °C/min

John G. Reynolds, Richard W. Crawford, and Alan K. Burnham,
University of California,
Lawrence Livermore National Laboratory,
Livermore, CA 94550.

Abstract

Kimmeridge, Phosphoria, La Luna, Teistberget, New Albany, Janusfjellet, Wenzen, Maoming, Fushun, Woodford, and three Green River oil shales were subjected to programmed-temperature pyrolysis at a heating rate of 10 °C/min using triple-quadrupole mass spectrometry as the detection method. Volatile compound evolution, including hydrocarbons, non-condensible gases, and heteroatomic compounds were monitored by on-line detection. As expected, the temperatures of maximum evolution rate (T_{max}) depended on the sample and the species evolving. The T_{max} values for generation of total light volatile organic compounds were between 442 to 472 °C, with the New Albany (eastern U.S. Devonian) giving the lowest values and Brotherson (Green River formation) giving the highest values. The heteroatomic species had T_{max} values which were slightly lower than those for hydrocarbon evolution. Non-hydrocarbon gas formation, particularly H_2S, CO_2, CO, and H_2O, was highly dependent upon the mineral matrix and mineral matrix-kerogen interactions of the shale.

Introduction

Locating oil in a formation, and predicting where generation will occur are relevant contemporary problems for geochemistry. We are studying the kinetics of oil generation through laboratory simulated pyrolysis of source

rocks to better address these problems.[1] To extend our data base, we have selected several oil shales and petroleum source rocks from various geographical locations, from both marine and lacustrine source types and subjected them to programmed temperature pyrolysis at various heating rates, from room temperature to 900 °C, using triple-quadrupole mass spectrometry (TQMS) as the detection method. This technique has been utilized previously for several studies on pyrolysis of oil shale,[2-5] tar sands,[6-8] and coal.[9]

TQMS is particularly suited for this type of study because it provides on-line, time-resolved analysis. By these experiments, we follow the evolution as a function of temperature of various light hydrocarbons, N-, S-, and O-containing compounds, and non-hydrocarbon gases. The pyrolysis profiles obtained allow determination of evolution range and T_{max}. Multiple heating rates allow determination of kinetic parameters for which the ultimate aim is extrapolation to geological conditions. This report presents the evolution behavior of several oil shales and petroleum source rocks at the heating rate of 10 °C/min. Selected preliminary results from this study were presented earlier.[10] In addition, the kinetics derived from multiple heating rates will be reported separately.

Experimental

Instrumentation. The TQMS utilizes both MS and MS/MS detection coupled with computer controlled acquisition which allows for the detection of over 40 components in 15 seconds.[11,12] In the MS mode, m/z 2 and m/z 12 to 125 were scanned. In the MS/MS mode only specific ions were scanned. These ions were selected based on unique parent-daughter combinations (total of 145 parent-daughters from 28 different parents). Four different source files were used (one each for m/z 2, MS, MS/MS, and MS/MS charge exchange) to insure maximum sensitivity and stability for all species. The parameters were cycled while acquiring data. Table 1 lists 33 selected pyrolysis gases and their various m/z combinations used for detection. Compounds analyzed for are C_1- through C_7-hydrocarbons, C_2- through C_5-volatile sulfur compounds, the non-condensible gases, H_2, CO, CO_2, H_2S, SO_2, and COS, as well as H_2O, CS_2, and several N- and O-containing compounds. In addition, Ar was

monitored for flow changes and instrumental drift using m/z 40, 20, 36/36. All profiles were corrected for this.

The species listed in Table 1 were detected by MS and MS/MS detection, or, in some cases, by both. In many of the MS cases, the species profile was a result of subtraction of interfering ions based on cracking patterns of the pure compound under the same conditions. The direct detection of methane was by monitoring m/z 16, but then subtracting out m/z 16 contributions from CO, CO_2, and H_2O. Direct detection of C_2H_4 was by monitoring m/z 28, with subtractions of contributions from other hydrocarbons, such as C_2H_6, C_3H_6, C_3H_8, etc. Hydrocarbon species above C_3H_6 were not corrected for other hydrocarbon fragmentation.

Several MS/MS combinations allow direct on-line unambiguous determination of species, where MS does not. For examples, m/z 16 includes fragments from CO_2, CO, H_2O, as well as CH_4, while the m/z 16/14 combination is only CH_4; m/z 44 includes CO_2 and C_3H_8, while the 44/29 combination gives C_3H_8 only. Table 1 also lists several MS/MS combinations that give unique determination of sulfur and nitrogen gases. For example, m/z 84 includes contributions from C_6H_{12} and thiophene. From the table, these can easily be separated by MS/MS combinations. H_2S was monitored by both m/z 34 and 34/32. Few species produce m/z 34 which would interfere.

Table 1 also shows the MS/MS combination for CO is m/z 28/84. m/z 28 has contributions which are also due to CO_2 and C_2H_6 fragments as well as C_2H_4. By replacing Ar with Kr in the collision chamber, selective charge transfer can be afforded by CO, but not the other species, therefore allowing unique determination of CO in the hydrocarbon matrix.[13]

Pyrolysis Experiments. In these experiments, the pyrolysis reactor was a 1/4 inch quartz tube holding approximately 0.5 g of shale, and was heated at a rate of 10 °C/min with a constant Ar sweep of 30 cm^3/min. In some cases, when the samples were finely powdered, quartz was used as filler material. The evolving components flowed into a trap kept at 140 °C. This allowed for light volatile hydrocarbon and heteroatom (N,S,O) compounds up to about C_8 to pass through to the mass spectrometer, while the heavy components were

retained. In addition to qualitative detection, several of the volatile components were also quantitated. The width of the evolution profiles indicate in most cases multiple activation energies. This will also be discussed in detail in the kinetics report.

The temperature of the sample was monitored by K-type thermocouples. These thermocouples were calibrated before and after each run with reference to an NBS standard. Care was taken not to expose them to radical cooling conditions above 200 °C. Thermal gradients across the sample in the reactor were also checked by multiple thermocouples in quartz test samples submitted to normal experimental conditions. No thermal gradient was detected in the test samples.

In addition to accurate temperature calibrations, hold-up in the system from the reactor to mass spectrometer was measured (using CO_2 calibration mixtures) and a correction factor of 5 °C was calculated based on sample heating rate. This correction was applied to all temperature values reported.

Most of the samples were also characterized by pyrolysis in a Pyromat II (Lab Instruments, Kenwood, CA) micropyrolysis instrument.[14] 15 mg of sample was held in a quartz tube in contact with a type K thermocouple. The sample was heated at a programmed heating rate, chosen to be 9.2 °C/min in this case for comparison to the TQMS results. The total pyrolysate is monitored with an adjacent FID detector operated at 550 °C.

Oil yields were also determined from autogenous flow pyrolysis. The method has been described in detail elsewhere.[15] Briefly, the sample was pelletized and heated at 2 °C/min. Evolving oils and gases exited through a stainless steel frit in the bottom of the reactor. The oil was collected in a graduated test tube.

Samples. Table 2 describes the shales examined in this study. Both marine and lacustrine samples and one terrestrial sample from several locations throughout the world were examined. Pyrolysis experimental conditions and errors were determined by multiple runs on Woodford (WDFD) and New

Albany (NAKY) shales. Less abundant samples were examined generally 1 or 2 times.

Sources of several of the shales have been described previously.[1,14,15] In addition, NAKY is from the New Albany formation; AP-24 (AP24), Government (GOVT), and Brotherson (BROT) are from the Green River formation. AP24 comes from the Anvil Points mine in the Mahogany zone in Colorado. GOVT comes from the 1634 m depth of the Government 33-4 well and BROT from the 2557 m depth of the Brotherson 1-23B4 well in the Uinta Basin, Utah. Both were provided by Shell Development Co.. GOVT contains 10% vitrinite and 5% exinite (DGSI, The Woodlands, TX). BROT comes from just above the oil window. Wenzen (WNZN) comes from the Lias ε formation, and was provided by J. Rullkotter (KFA); La Luna (LLNA) was provided by S. Talukdar (INTEVEP); Janusfjellet (JNUS), Teistberget (TSTB), and Kimmeridge (KIMR) were provided by B. Dahl (Norsk Hydro). JNUS and TSTB are outcrop samples from Svalbard, Norway. TSTB is a marine shale and JNUS is a terrestrial shale with some marine input. Phosphoria (PHOS) was provided by G. Claypool (USGS).

Two samples each of Maoming (MMNG) and Fushun (FSHN) shales were also examined. These samples were from the same formation but obtained from different sources. The samples appended with I were obtained from R. C. Rex, Jr. (Hycrude Corporation) and those appended with II were obtained from Zhang Shi Ko (Sinopec International).

Table 2 also lists qualitative identification of minerals by x-ray diffraction for the shales. A major phase has a height of 50 to 100% of the most intense peak; a minor phase is 10 to 50% of the strongest peak; trace components are <10%. Due to the different peak width and relative intensities, these designations are only descriptive. The clay to quartz ratio is derived from the relative peak height of the 4.46Å and 4.26Å peaks. The 4.46Å peak is common to all clay minerals. Smectite, illite, and kaolinite clay groups were identified according to the following ranges – 13-15Å, 8-10Å, and 7Å, respectively. The clay group peaks were typically broad and sometimes multifeatured. The other minerals were generally sharp and easily identified by pure compound patterns.

Table 3 lists selected chemical analyses of the shales studied. Some of these analyses have been reported previously.[1] All values except for ratios are % by wt of total sample. Autogenous oil yields have been reported previously.[15] C, H, and N were done on a Leco 600 analyzer, total S on a Leco SC 132 analyzer, S speciation was done by a modified ASTM D 2492-84 procedure (total S was done as above).

Of the shales listed in Table 3, Five (LLNA, WNZN, AP24, GOVT, BROT) are high carbonate shales, and four (KIMR, NAKY, WDFD, WNZN) have fairly high levels of iron-sulfide species. This agrees well with the qualitative relative abundances shown in the x-ray analysis (except for the sulfides for TSTB). It must be noted that x-ray analysis has the following caveats: very small particle size materials, amorphous materials, and materials at concentrations less than a percent generally are not observed.

The organic carbon levels vary from very abundant in MMNG II to very low levels in JNUST. The intensity of many species in the TQMS analysis is dependent upon this property. BROT yielded fairly noisy profiles partly because of its particular low level of organic C.

Results and Discussion

Hydrocarbon Evolution. The pyrolysis profiles for hydrocarbon evolution for many shales have a single prominent maximum with a temperature of maximum evolution (T_{max}) around 425 to 520 °C. The T_{max} value depended upon the hydrocarbon evolving and the particular shale. The evolution profiles were fairly sharp, except in methane evolution and isolated cases for higher hydrocarbons (see below).

Behavior of C_4^+ Hydrocarbons. Table 4 shows T_{max} values for the total light organics (TLO) evolved, and compares these values to T_{max} values for the $C_4H_9^+$ ion, the T_{max} measured by a Pyromat II micropyrolyzer, and by Rock Eval pyrolysis.[15] The T_{max} value for TLO comes from taking the total ion current of all the species evolving (which pass through the 140 °C trap) at a specific temperature and subtracting the ion current contributions from non-

hydrocarbon gases (SO_2, CO_2, H_2S, HS, S, H_2O, NH_3, H_2) and the carrier and analysis gases (Ar, Kr). The $C_4H_9^+$ ion is from monitoring m/z 57 and is a result of fragmentations from most hydrocarbons of C_4H_{10} and higher. It is meant to be a indicator of these larger noncondensed alkyl hydrocarbons as opposed to only butane. The Pyromat II and the Rock Eval analyses were included to give a comparison measurement of total hydrocarbons which is not based on MS methods and are more common in the literature. For a specific sample, the values of the Pyromat II technique are generally slightly lower than the TLO T_{max} values from the TQMS (NAKY, JNUS, FSHN I are the exceptions), but are still in good agreement. The Rock Eval T_{max} values are all lower than the corresponding TLO T_{max} values, even though the Rock Eval heating rate is nominally 25 °C/min. (The Rock Eval instrument is calibrated to a relative temperature scale that is about 35 °C lower than the true temperature.[16]) Even so, the values correlate well giving a linear best fit of TLO T_{max} (°C) = -18.4 + 1.093 [Rock Eval T_{max} (°C)], with an R^2 = 0.86 for 11 data points. The linear relationship suggests the TLO and Rock Eval can be used for similar purposes.

Comparing T_{max} values for TLO, the shales can be grouped by type. The marine shales have T_{max} values between 442 and 458 °C and the lacustrine shales between 455 and 472 °C. (The $C_4H_9^+$ T_{max} values behave similarly.) The same grouping is observed for the Pyromat II and Rock Eval T_{max} values, but with slightly different temperatures ranges: Pyromat II, marine -- 441 to 456 °C, lacustrine – 451 to 467 °C; Rock Eval, marine -- 425 to 432 °C, lacustrine -- 433 to 448 °C. TSTB has T_{max} values which are higher than expected based on the T_{max} values of the other marine shales. This could be due to weathering, because TSTB is an outcrop sample.

Besides the grouping by shale type, the Green River formation stands separately in the table, having T_{max} values for TLO much higher than other shales. In addition for both TLO and Pyromat II values JNUS has T_{max} values which are comparable to the lacustrine T_{max} values. JNUS is a terrestrial shale with marine influence.

The TLO T_{max} values and corresponding $C_4H_9^+$ T_{max} values are similar, in general. NAKY has the lowest T_{max} for both sets, while BROT has the highest

for both sets. The biggest differences between the two sets are for WDFD, where the T_{max} for TLO is 8 °C lower than for the $C_4H_9^+$ fragment. In some cases (PHOS, GOVT, MMNG II) the T_{max} for TLO generation is higher than the T_{max} for $C_4H_9^+$ ion, but in all other cases it is the same or lower.

Behavior of C_1-C_4 Hydrocarbons. Figure 1 shows CH_4, C_2H_6, C_2H_4, C_3H_8 and C_4H_{10} evolution profile sets for the 15 shales studied. The legend identifies the species and shows the total evolution of the species, in cm^3/g (at 298 °C) of total organic carbon (TOC), by integration of the profile. Also shown are the T_{max} values for each species. Because of the overlap of profiles, the T_{max} values and total evolution are listed in Table A1 in the Appendix, for clarity.

Figure 1 shows that the profile sets look approximately the same for all samples. From this, some generalizations can be made about the evolution of the five hydrocarbons: 1) T_{max} values range from 429 to 513 °C with T_{max} value for CH_4 almost always being the highest for each shale, 2) for a specific shale, CH_4 usually is produced in the largest volume (45 to 70 vol % of total C_1 - C_4 quantified), and 3) all shales produce roughly the same total volumes of C_1-C_4 quantified.

Figure 1 also shows trends which tend to follow the marine and lacustrine grouping. The marine shales appear to have a shoulder on the low temperature side of the CH_4 maximum which corresponds roughly with the T_{max} of the larger hydrocarbons. KIMR and the lacustrine shales do not exhibit this. For the lacustrine shales, the T_{max} values of the CH_4 peaks are close to the T_{max} values for the larger hydrocarbons, but no low temperature side shoulder is observed. It appears that the low temperature shoulder is now the main peak for lacustrine shales, and CH_4 co-evolves with the other species, while in the marine shales, CH_4 evolution lags.

Although KIMR has T_{max} values for the larger hydrocarbons which are lower than the T_{max} value for CH_4, contrary to the behavior of the other marine shales, no low temperature side shoulder appears on the CH_4 profile. And contrary to the behavior of the lacustrine shales, MMNG I and II have a large discrepancy between the T_{max} values for CH_4 and the larger hydrocarbons, but do not exhibit a low temperature side shoulder.

To further demonstrate some of these trends which show a distinction between marine and lacustrine shales, Figure 2 shows the behavior of T_{max} values of the individual species measured by the TQMS with reference to the Rock Eval T_{max} values given in Table 4. MMNG I and FSHN I Rock Eval T_{max} values have not been measured, so these comparisons are absent in Figure 2. Methane (as indicated by TLO - CH_4 T_{max} values) shows two groupings consistent with the above observations. The marine shales have a much larger difference from the TLO than the lacustrine shales. MMNG II is an exception, bridging both groups. This same behavior is seen for C_2H_4 and C_2H_6 (both not shown), but with decreasing deviation from the TLO value. This decrease is dramatic enough that the C_3H_8 values (as indicated by TLO-C_3H_8 T_{max} values in Figure 2) are almost randomly scattered about the zero line.

Figure 2 also shows the behavior of C_2H_4 - C_2H_6 T_{max} values as measured by TQMS with respect to the Rock Eval T_{max} values. The marine shales generally show a much bigger difference than the lacustrine shales. Once again, MMNG II is the anomaly.

Table A1 in the Appendix lists the T_{max} values for several hydrocarbons monitored. The following summarizes the results: 1) the T_{max} values for C_2H_4 and C_2H_6 are all higher than the corresponding T_{max} values for TLO (these differences are not very large for lacustrine shales), 2) the differences in T_{max} values of C_2H_4 compared to C_2H_6 values are much larger for marine shales than lacustrine shales (see Figure 2), 3) T_{max} for C_3H_8 evolution is very similar to the T_{max} values for TLO, 4) T_{max} value of C_4H_{10} is generally the lowest for all the hydrocarbons quantified, and 5) the three Green River shales exhibited little variation in the T_{max} values throughout the series while all the other shales exhibited considerable variations.

Figure 1 also shows many of the shales have a shoulder on the high temperature side of the CH_4 profile, approximately 100 °C above the T_{max} value. This shoulder is observed in all the lacustrine shales, but not systematically observed in the marine shales or JNUS, indicating, in these latter cases, the reactions causing this evolution are probably occurring at

temperatures closer to the major CH_4 evolution. NAKY has a gradual tail; WDFD, WNZN and TSTB have a definitive shoulder. The broadness of JNUS, PHOS and LLNA suggests equal intensity shoulder and main peak.

Visible in some of the profiles in Figure 1 is a small maximum at temperatures around 800 °C, probably due to gasification of char, where some of the methyl groups pyrolyze as CH_4 rather than CO.

The low and high temperature shoulders on the methane profile suggest different types of mechanisms or sources for methane evolution, particularly when looking at differences between lacustrine and marine shales. The low temperature shoulder on the marine shales corresponds closely with the T_{max} values from the other hydrocarbons suggesting it is directly related to primary hydrocarbon evolution. This is also suggested by the T_{max} value for CH_4 in the lacustrine shales. However, in the marine shales, the T_{max} for CH_4 is shifted much higher suggesting an alternative, secondary mechanism produces the majority of the CH_4 evolved. This secondary mechanism could be char demethylation reactions which have been considered responsible for the high temperature side shoulder seen in lacustrine shales. This behavior difference suggests that most of the kerogen from lacustrine samples (except MMNG) is converted to oil, while most of the kerogen in marine shales is converted to aromatic, coke-like residue. The temperature of evolution of this residue is expected to be higher because aromatic-methyl groups have higher bond energies than aliphatic bonds and do not have the option of β-scission as longer alkyl-aromatic structures.

General Behavior of Hydrocarbons. Table A2 in the Appendix lists the T_{max} values for hydrocarbons monitored but not quantified. Figure 3 shows these T_{max} values along with the T_{max} values of the quantified hydrocarbons as the difference from the corresponding TLO T_{max} values. Generally, for almost all the shales, the biggest positive difference is with CH_4 and the biggest negative difference is with C_4H_{10}. There are exceptions (AP24 for methane; GOVT and KIMR for C_4H_{10}). The T_{max} values of the higher hydrocarbons are fairly close to those of the corresponding TLO. Some trends in the T_{max} values of the non-quantified hydrocarbons compared to the T_{max} values of the TLO are: 1) C_5H_{10} are about the same, 2) C_5H_{12}, C_6H_6, and C_7H_{10} are lower, and 3) C_6H_{12}

appear higher. C_7H_8 T_{max} values compared to corresponding TLO T_{max} values show some behavior based on shale type -- lacustrine, higher; marine, about the same.

In many of the above generalizations about T_{max} values MMNG I and MMNG II appear to have anomalous properties for the shale type. MMNG I and II are classified as lacustrine shales. However, consistently C_2H_4, C_2H_6, ethene/ethane ratio and other properties are more like marine shales. The reason for this behavior is not known.

Our results for T_{max} values are similar to earlier results for eastern U.S. Devonian shale,[2,17] Chinese shale,[2] and Green River shale.[2,18] Our values are generally higher because of the faster heating rate, but there also appears to be minor differences from the earlier work[17-19] due to improvements in techniques. In addition, Table 4 shows the T_{max} values for C_2H_4 and C_2H_6 evolution are consistently higher than for total evolution, in agreement with previous results[2,17].

For CH_4, the AP24 value is 13 °C higher than the T_{max} reported earlier at a 4 °C/min heating rate, which is consistent with the higher heating rate.[18] The T_{max} for NAKY also agrees with values for eastern U.S. Devonian shales heated at 4 °C/min reported by Coburn[17] and Oh et al.[2] We also observe a shoulder on the low temperature side of the prominent maximum at about 470 °C. This is in agreement with Oh et al. who observed the shoulder at 450 °C and assign it as probably due to CH_4 generation from kerogen pyrolysis. Oh et al. also reports the MMNG I and FSHN I shales having T_{max} at 500 °C. These values are higher than those in Figure 1 which would not be expected at the lower heating rates. Because of the broad nature of the CH_4 peak, T_{max} values are difficult to assign when the signal-to-noise is not good. In addition, they observed shoulders around 600 °C, consistent with Figure 1.

Our hydrocarbon gas yields agree very well with previous results. Our methane yield of 34.4 cm^3/g TOC for AP24 is the same as the 34 cm^3/g TOC determined earlier by conventional pyrolysis-mass spectrometry.[18] We do not quantitate unsaturated C_3- and C_4- and any C_5-hydrocarbons, but we can estimate from Fischer Assay yields[20] and closed system pyrolysis.[21] Assuming

a propene/propane ratio of 0.8 and a butene/butane ratio of 1, our calculated C_2-C_4 yield of 101 mg/g TOC for AP24 agrees well with that determined by Fischer assay.[20] Our hydrocarbon gas yields for KIMR are very similar to results of Espitalie et al.[16] for the pyrolysis of a Kimmeridge (type II) kerogen from the Viking group by a modified Rock Eval I system at 4 °C/min heating rate. Their methane yield (19.8 mg/g TOC) was nearly identical to ours (19.2 mg/g TOC). Our total C_2-C_4 yield was estimated to be 43 mg/g TOC. This is very similar to their C_2-C_5 yield of 36 mg/g TOC. Also, JNUS is primarily terrestrial or Type III organic matter, and its pyrolysis yields are similar to both the shales but also to the pyrolysis yields for Argonne[9] and Brent[16] coals, also type III materials. Espitalie et al. state that the amount of gaseous hydrocarbons evolving were similar no matter what type of source was being considered. With our larger group of shale samples, we find more variation in yields of C_1-C_4. At the extremes, AP24 gives nearly three times as much C_1-C_4 as KIMR and MMNG. JNUS gives an average C_1-C_4 yield, even though its HI is only 160 mg/g TOC, which means that it is producing proportiionately less C_5^+ material.

Espitalie et al.[16] monitored the hydrocarbon evolution grouped in the following classes, C_1, C_2-C_5, C_6-C_{15}, C_{15+}. They concluded the T_{max} values for each class increased as the molecular weight of the class decreased. Our results agree mostly with this behavior. We see a decrease in T_{max} as the carbon chain-length increases, with generally a minimum T_{max} at C_4 (see Figure 3), and with not much change for hydrocarbons larger than C_4.

Carbon Dioxide Evolution. Figure 4 shows the CO_2 evolution profiles for the shale examined. The scales are normalized for ease of display. Also listed in parentheses is the the total evolution for each shale in cm^3/g of shale. Generally, the shales can be grouped into three types: 1) high carbonate shales (LLNA, WNZN, BROT, GOVT, TSTB, and AP24), 2) low carbonate-mineral shales (PHOS, WDFD, KIMR, and JNUS), and 3) high siderite-mineral shales (MMNG I, MMNG II, FSHN I, and FSHN II). Clearly, the high carbonate shales evolve much more CO_2 than the low carbonate shales and siderite shales. MMNG II and FSHN II are almost identical to MMNG I and FSHN I so are therefore not displayed.

The evolution pattern of the high carbonate shales, Figure 4A, shows generally a very small maximum around 400 to 450 °C, and prominent evolution in the 650 to 900 °C range. The former has been tentatively assigned in oil shales and tar sands to be due to the decomposition of oxygen-containing organic compounds, such as carboxylic acids and salts, and ketones.[6-8,17,18,22] The high temperature evolution which dominates the profiles has been assigned to carbonate mineral decomposition, equation (1), where M represents Ca, Mg, and Fe in calcite, dolomite, and ankerite, respectively:

$$MCO_3 \rightarrow MO + CO_2 \quad (1)$$

Table 2 lists BROT, WNZN, LLNA, and AP24 having calcite and/or dolomite as the major mineral. GOVT and TSTB are the only other shales that have any appreciable carbonate minerals (MMNG and FSHN will be discussed below). Independent acid carbonate determinations listed in Table 3 confirm this for AP24, WNZN, BROT, LLNA, GOVT, and TSTB. These CO_2 evolution results are in excellent qualitative agreement with the x-ray and acid carbonate results and previously published results on AP24 and NAKY shales.[2,17,18]

The evolution profiles for the low carbonate shales, Figure 4B, are very complex and a complete analysis is beyond the scope of this paper. PHOS is dominated by CO_2 evolution at low temperature which may be due to organic decomposition or CO_2 retained by minerals. KIMR has a trace of dolomite in the mineral analysis which appears to evolve around 700 to 800 °C. The evolution profiles of the Chinese shales, Figure 4C, are dominated by the CO_2 evolution from the decomposition of siderite, $FeCO_3$, as verified by a TGA determination on the pure mineral.

Figure 4D shows the CO_2 profiles for the high and the low mineral shales for the temperature range from 300 to 600 °C. (The FSHN and MMNG samples were excluded because of their intense CO_2 evolution in this range.) Although the evolution behavior is very complex, in most cases, CO_2 evolution correlates well with water and H_2S evolution in the temperature range around 475 to 600 °C. Some of this evolution can be described by certain

reactions. H_2S is known to react with iron-bearing carbonates[22,23] at fairly moderate temperatures by equation (2):

$$FeCO_3 + H_2S \rightarrow FeS + CO_2 + H_2O \quad (2)$$

Shales which generate reasonable levels of H_2S corresponding to CO_2 evolution at the same temperature are BROT, GOVT, WNZN, TSTB, PHOS, AP24, and NAKY. Evolution of water from clay could also enhance CO_2 evolution because water enhances carbonate decomposition.[24]

Below 475 °C, CO_2 evolution appears at similar temperatures as hydrocarbon generation. The origin of this CO_2 is not certain, but model compound pyrolysis experiments with Ni 2-ethylhexanoate and Fe stearate indicate CO_2 occurs with hydrocarbon evolution. This suggests the origin of CO_2 in the shales in this temperature range could be due to the decarboxylation of carboxylic acids and salts as shown in equation (3):

$$RCH_2CH_2COOH \rightarrow CO_2 + RCH_2CH_3 \quad (3)$$

This is most evident in AP24, PHOS, KIMR, WDFD, WNZN, and GOVT.

Figure 4 also shows the total evolution for CO_2 generation in cm^3/g of shale. Clearly, the high carbonate shales evolve the most CO_2, predominantly from carbonate breakdown. The low CO_2 yield for the siderite shales are consistent with the x-ray analysis of Table 2.

Carbon Monoxide. Figure 5 shows the CO evolution profiles (normalized) as a function of pyrolysis temperature for the shales studied. No evolution of CO is seen below 300 °C, after which evolution begins. In most of the profiles, a small maximum is evident around 410 °C and falls in the range of hydrocarbon evolution due to kerogen breakdown, pyrobitumen and bitumen cracking reactions. The chemical species responsible for this evolution is not certain, but pyrolysis of the model compounds discussed above for CO_2 evolution, also produced CO (a ratio of 1.4/1, CO/CO_2 for Ni 2-ethylhexanoate) in the same temperature range as hydrocarbon evolution.

This suggests the origin of CO in this temperature range may be the decarbonylation of carboxylic acids and salts[21] as shown in equation (4):

$$RCH_2CH_2COOH \rightarrow CO + H_2O + RCH{=}CH_2 \quad (4)$$

In shales containing iron carbonates, CO could also be generated in this temperature range by the decomposition of the iron carbonate forming Fe_3O_4, CO_2 and CO. In addition, metal carbonates could also react with hydrogen donors (possibly from organics) to form the metal oxide, CO, and H_2O.

The majority of the CO evolved occurs above 600 °C, and is probably not directly related to hydrocarbon generation, although stable aromatic ethers in char could decompose as the char breaks down further. This high temperature CO could have a variety of origins.[18,25] For high carbonate shales, equation (5):

$$CO_2 + CH_x \rightarrow 2CO + (X/2)H_2 \quad (5),$$

accounts for almost all of the CO and CO_2 chemistry. For the low carbonate, high clay shales, equation (6):

$$H_2O + C \rightarrow CO + H_2 \quad (6),$$

becomes more important. However, in both cases, equation (7):

$$CO + H_2O = CO_2 + H_2 \quad (7),$$

must be considered, although probably with less modifying effects for the high carbonate shales than the low carbonate shales.

The relationship of equations 5 through 7 is further demonstrated by comparing the total CO_2 production as measured by the TQMS and comparing it to the CO_2 levels as measured by acid carbonate determinations (Table 3). Table 5 lists these values for each shale in wt percent of shale. The total production was measured utilizing the relationship for CO_2 and CO in equation 5 ($CO_{2total} = CO_{2measured} + (1/2)CO_{measured}$). Clearly, in the high

carbonate shale cases, the CO_2 production is dominated by mineral decomposition, equation 1, and therefore equation 5 is significant in CO production. For the siderite shales, total CO_2 production is also dominated by mineral decomposition, and equation 5 is also significant for CO production. For the low carbonate shales, the behavior is not as clear. The CO_2 balances based on acid carbonate determinations are, in some case, very poor. The values for total CO_2 production are much higher than predicted by acid-carbonate measurements, suggesting that CO_2 production other than that from carbonate mineral decomposition is important, and CO contributions through equation 6 are not the only source. Equations 6 and 7 are probably important sources for CO and CO_2 for these shales.

The CO_2 and CO profiles for each shale were compared to further understand the relationship between the two species. The high carbonate shales also had high CO evolution at high temperatures (Figure 6A shows GOVT as an example). The low carbonate shale exhibited typical char gasification chemistry at high temperatures. The CO evolution increases while the CO_2 evolution decreases (Figure 6B shows NAKY as an example).

Hydrogen. Figure 7 shows the H_2 evolution profiles as a function of temperature for the shales studied. The profiles show no hydrogen evolution before approximately 350 °C. Several maxima are seen above this temperature, depending upon the oil shale. For AP24, BROT, MMNG I, MMNG II (not shown), FSHN I (not shown), FSHN II, the best defined maximum is in the range of 460 to 490 °C. This is also evident as a broader maximum for all the other shales. The T_{max} value of this peak is listed in the figure, and the percentage of the total H_2 evolution accounted for by this peak is shown in the parentheses. This peak accounts for 17 to 42% of the total evolution and has been attributed to kerogen breakdown, aromatization, cracking, and dehydrogenation reactions of non-volatile bitumen. The differences between this T_{max} value and the corresponding T_{max} value for TLO (see Table 4) depended upon the shale, varying from 3 to 48 °C. This type of maximum has been observed before in oil shale,[2,17-19] and tar sands[6-8] pyrolysis.

Figure 7 also shows that the majority of the hydrogen is evolving above this maximum. This hydrogen can be attributed to several reactions, depending upon the temperature and the shale. The H_2 evolving in the 500 to 650 °C range has been assigned previously[18] to char pyrolysis reactions where the residual kerogen, and non-volatile bitumen are further decomposing yielding surface coke, H_2, and CH_4 (see above discussion). H_2 evolving above this can have additional contributions from a variety of secondary reactions including the char-gasification reactions, and the water-gas shift equilibrium, equations (5) to (7).

From Figure 7, the lacustrine shales appear to behave differently from the marine shales, where as for hydrogen, the lacustrine shales have a generally sharp low temperature maximum, while the marine shales do not. Except for this behavior, and few other individual differences, the profiles generally behave the same. Some of these differences are: NAKY, JNUS, and LLNA appear to have two low temperature maxima, PHOS has a very sharp low temperature maximum, and a very low percentage of the total hydrogen evolving in the hydrocarbon evolution range.

Water Figure 8 shows the water evolution profiles for all the oil shales studied. Only one sample each from the FSHN and MMNG samples are shown, because the others are essentially identical. All oil shales exhibited water evolution which reflects hydrated mineral decomposition as well as other sources. In general, water evolution during oil shale pyrolysis can be broken into five broad categories:[26] 1) free water, 2) water from inorganic hydrates, 3) water from reactions of H_2S with iron compounds, 4) water from elimination of organic oxygen, and 5) equilibrated water and from mineral dehydration.

Free (surface) water. Virtually all the oil shales have evolution slightly above 100 °C, and in some cases, this evolution accounts for a substantial percentage of the total water evolved (PHOS, 41%; BROT, 27%; FSHN, 18%). Only NAKY, WNZN, and MMNG I (not shown) do not show significant water evolution at this temperature. These shales were heated slightly above 100 °C before the experiment started, prematurely releasing this water. Table 2 shows many of the shales contain clay minerals (illite, montmorillonite, and

mixed clays) which release surface moisture upon heating,[27] and are most likely responsible for this evolution.

Inorganic Hydrates. Figure 8 shows several of the shales evolve water in the range of 150 to 400 °C (JNUS, TSTB, WNZN, MMNG II, KIMR, LLNA, WDFD, PHOS). This type of water has been attributed to: 1) sulfur-oxygen anions from pyrite oxidation;[26,28] (all shales except the MMNGs have at least some pyrite), 2) analcime decomposition (prominent in the Green River formation shales), and 3) quartz derived (all shales have some quartz and quartz was used as filler material in the reactors). PHOS, LLNA, FSHN II TSTB, WNZN, and GOVT also have peaks at approximately 235 °C. The source of this peak is unknown, but could be due to the dehydration of palygorskite (attapulgite) or goetite (FeOOH).[27] The former is difficult to distinguish by XRD from illite and the latter may be present based on the appearance of a broad shoulder at d = 4.18Å on the quartz peak.

Acid-Base Chemistry. Figure 8 shows, for most of the shales, major evolution of H_2O occurs in the range of 400 to 600 °C. Equation (2) indicates water as well as CO_2 are evolved during H_2S capture by iron minerals. However, these reactions occur in the same region as clay dehydration, so it is difficult to determine how much they influence the observed water evolution profiles.

Organic Oxygen. Dehydration of organic matter has been shown to be a minor contributor to water evolution from oil shale pyrolysis.[26] Durand-Souran et al.[29] found that isolated, immature kerogens of all types evolve water over a broad temperature range from 100 to 500 °C. For type III kerogens, it was also found that the low-temperature water diminished with maturity, so most of the water evolved in the 350 to 500 °C range. Similarly, Burnham et al. [9] found that the maximum water evolution rate from low rank coals heated at 4 °C/min came in the 400 to 500 °C range. Because the high mineral content of our samples, it is difficult to know how much of the water signal in this region is due to organic pyrolysis. LLNA, WDFD, NAKY, and to a lesser extent, PHOS, have fairly well defined maxima around 440 °C, probably due to organic decomposition.

Mineral Dehydration Water. Water evolution above 550 °C is often complicated by complex reaction chemistry, such as the water-gas shift reaction (and other high temperature reactions which feed it), equation (7), and the water-char reaction, equation (6). However, for many of the oil shales studied, evolution around 500 to 650 °C can be assigned to the dehydration of clays, particularly illite and kaolinite.[26] For the Chinese shales, the prominent maximum around 520 °C is probably due to primarily kaolinite dehydration, with contributions from illite, smectite and possibly halite. TSTB, WDFD, WNZN, and LLNA have evolution maxima around 540 °C which are probably due to the dehydration of kaolinite. In KIMR, JNUS, BROT, NAKY, GOVT, and PHOS, the evolution maxima around 575 °C are primarily due to decomposition of illite. BROT and WDFD probably have contributions due to smectite also.

In addition to these clays evolving water around these temperatures, the $\alpha \rightleftharpoons \beta$ transition of quartz at approximately 560 °C should be considered. Even though quartz is the principal mineral component of most of these shales, the $\alpha \rightleftharpoons \beta$ transition generally produces very little water, and the clays have very intense evolution around this temperature, so the transition may not be evident.

Also shown in Figure 8 are the total amounts of H_2O evolution in cm^3/g of shale. These values are the highest for any evolving species quantitated. Specifically, of all the shales, MMNG I (not shown) exhibits the most water evolution. This follows from the mineral analysis in Table 2 where the clay mineral kaolinite is one of the prominent minerals of the shale. Likewise, MMNG II, PHOS, FSHN I (not shown), and KIMR all evolve large amounts due to hydrated clays minerals being prominent. Water evolution amounts in other shales vary, based primarily on the hydrated clay content. WDFD, which evolves the least amount of water of the shales listed, has only trace quantities of the hydrated clays. LLNA also follows this trend.

The three Green River formation shales do not show the same distributions for water evolution. AP24 derives most of the total water from analcime decomposition; GOVT attributes most of its water from illite or clay

decomposition; BROT has major contributions from both the clay decomposition and high temperature reactions.

Hydrogen Sulfide. Figure 9 shows H_2S evolution for the shales studied divided into 3 groups -- shales with: 1) a prominent maximum around 550 °C, 2) a prominent maximum around 420 °C, and 3) both maxima (Figures 9 A, B, and C, respectively). These profiles are in good agreement with the H_2S profiles reported previously for Green River[3] and eastern U.S. Devonian oil shales.[17]

The evolution of H_2S in oil shale pyrolysis is generally governed by three phenomena[30,31]: 1) decomposition of FeS_2, 2) the decomposition of organo-sulfur compounds, 3) capture of H_2S by iron-containing minerals, usually carbonates. Pyrite decomposition is complicated, being affected by the ability of the surrounding medium to remove S from the grain surface.[22] In a vacuum or inert gas, it is removed as S_2. In oil shale, it is removed principally as H_2S after reaction with organic hydrogen donors or water. Pyrite grain size also affects the rate via the surface-to-volume ratio.

These processes combine in complicated and poorly understood ways to produce the profiles in Figure 9. The lowest temperature process occurs at about 200 °C and is most evident in samples AP24 and MMNG I. The precise source of this peak is unknown. For Green River formation samples, the size of the peak varies from sample to sample.[32] The peak is also not present under self-purging conditions unless the sample is treated with HCl to remove carbonates, indicating the importance of secondary capture reactions.[32] The peak at 400 to 450 °C is primarily organic if the sample is well swept[3] or if pyrite is not present, as in tar sand bitumen and asphaltenes.[33] In the present experiments, the H_2S T_{max} value was within 10 °C of the T_{max} values of thiophene and methylthiophene. However, finely dispersed pyrite can react with hydrogen donors to contribute to this peak.[30] Comparison of the AP24 profile with previous results at other pyrolysis conditions[3,30,31] suggests the pyrite may have reacted to some extent under the present conditions. A large, sharp peak at 520 to 550 °C is observed for about half the samples. This is due to pyrite decomposition occurring roughly in this temperature range even when hydrogen donors to convert S_2 to H_2S are

absent. There may also be minor H_2S contributions above 500 °C from pyrolysis of the residual kerogen (char) as indicated by the CH_4 and H_2 profiles.

We were unsuccessful at understanding the behavior of the overall H_2S yields for the samples. The total H_2S generation correlated roughly with the total S in the sample. However, it ranged from 1 to 56% of the shale S for MMNG II and WDFD, respectively. The low MMNG II value is undoubtedly caused by capture of H_2S by siderite. This reaction can attain scrubbing efficiencies of more than 95% for H_2S and mercaptans under self-purging conditions,[22] although it does not appreciably affect thiophene generation. We did not detect significant quantities of S_2, but it is not likely the free S could pass through the trapping system. The upper limit may correspond to FeS as a final product. The percentage of H_2S evolved in the second peak correlated generally with the pyritic/organic S ratio calculated from Table 3, although there was much scatter. Both AP24 and FSHN II fall on the low side of this correlation, possibly indicating capture by iron-bearing minerals. LLNA had the smallest percentage contribution at 500 to 550 °C, probably because of its high organic S content. In PHOS, a shoulder rather than a distinct peak is observed in the 500 to 550 °C region.

Carbonyl Sulfide. In all the shales examined, at least some COS evolved. Table 6 lists the T_{max} values for these maxima. TSTB evolved some COS, but the noise was too great to provide any meaningful data. Primarily, three evolution ranges are observed with T_{max} values in the range of: 1) 350 to 450 °C, 2) 525 to 550 °C, and 3) above 750 °C. The evolution temperature ranges suggest some precursors. The T_{max} around 350 to 450 °C is in the range of hydrocarbon evolution due to kerogen pyrolysis and bitumen cracking. The T_{max} around 535 to 570 °C is in the range of FeS_2 decomposition. FeS_2 is known to react with CO to produce COS.[34] All the shales (except GOVT) which exhibit this maximum also have very high concentrations of FeS_2 (see Table 3). In many of the cases, this maximum is also at the same temperature as maxima for the evolution of H_2S and CS_2, suggesting complicated gas-shift chemistry may also be important. This COS behavior has been seen previously in the programmed temperature pyrolysis of Green River shales[3]

and several types of coals,[35] suggesting chemistry which is not dependent on organic matter type.

The high temperature evolution maximum is in the range expected for gas-shift reactions relating COS, H_2O, CO_2, H_2S, and CS_2. These reactions, along with the water-gas shift reaction, complicate the behavior of COS as well as CO_2, CO, H_2S, and H_2 at temperatures above 550 °C. As a result, H_2S is also expected to evolve at high temperatures. This is barely seen in BROT, KIMR, MMNG I, and PHOS profiles shown in Figure 9.

Carbon Disulfide. The high FeS_2 content shales also exhibited evolution of CS_2, with T_{max} values very close to the T_{max} values for H_2S evolution assigned to primarily FeS_2 decomposition (T_{max}, in °C, for CS_2 evolution: KIMR, 544; NAKY, 535; WDFD, 536; WNZN, 541; JNUS, 546; TSTB, trace amounts at 550). This has been seen previously for Green River shales[3] and several coal types.[35] This could be a result of the iron in FeS_2 being reduced by carbon, which is said to occur in the presence of organic compounds at temperatures as low a 250°C to 300 °C.[36] It has also been suggested from quantitative measurements of S in coals below 700 °C.[37]

Another source of the CS_2 could be through the gas-shift reactions which are known to occur at temperatures between 350 °C and 900 °C.[38] H_2S (Figure 9) and COS (Table 6) show co-evolution at the same temperatures as CS_2 evolution. Even KIMR has a small maximum in the CS_2 profile at 450 °C, which corresponds to intensity in both the COS and H_2S profiles. TSTB has a trace of CS_2 evolving, and has a trace of COS with a dominant H_2S maximum at the same temperatures. Previous results on coal show as yields increase for COS by varying pyrolysis parameters,[35] CS_2 yields decrease, also supporting gas-shift chemistry.

Sulfur Dioxide. We observed unambiguous, but unquantified signals indicating SO_2 evolution from all samples but BROT, TSTB, WNZN, and JNUS. The profiles were varied and frequently multifeatured. Common maxima were at approximately 310, 400, and 510 °C. The evolution may come from both organic and inorganic sources. SO_2 has also been observed from tar

sand bitumen[7] supporting the conclusions of Whelan et al[39] that organic matter may yield SO_2 upon pyrolysis.

Heteroatomic Compounds. Several S-, N-, and O-containing compounds also evolved during the pyrolysis of the oil shales. Of all these compounds, methylthiophene generally produced the most intense signal due to the amount generated of the species and favorable MS/MS response factors.

Thiophenes. Figure 10 shows the methylthiophene evolution profiles as a function of pyrolysis temperature for most of the shales studied. FSHN II and MMNG II are the same as their I counterparts, and therefore are not shown. Methylthiophene generation was not detected from JNUS, probably because of its extremely low organic content. The profile behavior is very similar to that of the hydrocarbons, where maximum evolution occurs in the region of hydrocarbon generation. Table 7 lists the T_{max} values and quantitation in cm^3/g TOC for methylthiophene. In general, the T_{max} values are much lower than the corresponding T_{max} for TLO listed in Table 4. However, there appears no grouping according to shale type. NAKY exhibited the smallest difference (9 °C), while KIMR exhibited the largest (28 °C). This evolution behavior for methylthiophene and other heteroatomic species has been seen before for AP24, NAKY,[5] MMNG,[2] KIMR,[1] and FSHN[2] oil shales, and tar sands.[6-8]

Thiophene, as well as methylthiophene, was detected and quantitated. Table 7 lists these values also. JNUS and BROT did not exhibit evolution of thiophene gas, and the thiophene data for the two MMNGs is at best marginal. However, due to variations in the sensitivity of the MS/MS experiments, we suspect that thiophene and other S gases are probably being evolved for these shales also.

The T_{max} values for thiophene, when observed, are all much lower than the T_{max} values for the TLO listed in Table 4, ranging from 7 °C lower (MMNG I) to 42 °C lower (GOVT) and follow the behavior of methylthiophene. It should be noted, identifying the T_{max} value for thiophene requires more smoothing of the evolution maximum than in the methylthiophene case, which could possibly introduce some errors in these values. The two

MMNGs are the extreme of this problem, and the large difference in the T_{max} values can probably be attributed to noise.

Generally, the T_{max} values in Table 7 exhibited no grouping according to shale type. Not surprisingly, however, the quantities of methylthiophene evolution seem to follow the organic S content and the org S/org C ratio shown in Table 3. Figure 11 shows org S/org C ratio vs methylthiophene content. The amount of methylthiophene correlates well ($r^2 = 0.8$) with both the org S/org C ratio in the shale and the total S content of the oil generated at 2 °C/min. KIMR, PHOS, LLNA, and WNZN exhibited the largest amounts of methylthiophene evolved, and have the largest org S/org C ratios. In contrast, the lacustrine shales all exhibit only small amounts of methylthiophene evolved and correspondingly have the lowest org S/org C ratios. These results agree with the contention methylthiophene is representative of the S-containing products formed during pyrolysis of these oil shales and that they come from S-containing moieties in kerogen.[40,41]

Flash pyrolysis studies on several of the oil shales presented here have revealed certain types of S-containing compounds in the pyrolysate, implicating more complicated S-containing structures in the kerogen as precursors. In the flash pyrolysis (610 °C for 10 sec) of kerogen extracts of Phosphoria Retort (type II-S) shale, the primary liquid and gas S-containing products (other than H_2S, COS, and SO_2) were the alkylthiophenes and alkylated benzothiophenes.[41] Minor products were thiolanes and thiolenes. These same products, although in different distributions, were found for the flash pyrolysis of kerogen extracts of LaLuna, Kimmeridge, Woodford, and New Albany (type II), and Green River (type I) shales.[41] Several proposed precursors have the thiophenic or analogous structure incorporated in the kerogen structure. The pyrolysis products are generally formed by the scission of alkyl bonds as mentioned above. The thiophenic structure itself does not breakdown readily to form H_2S. This gas is probably formed by sulfide and disulfide bridges thought to be links in the kerogen structure.[40,42] Artificial maturation experiments, followed by flash pyrolysis of kerogen extracts of LaLuna oil shale also show a large abundance of alkylthiophenes and very low concentration of alkylated benzothiophenes in the pyrolysate, also suggesting thiophenic-type precursors in the kerogen structure.[43]

We monitor only thiophene and methylthiophene in the gas phase, and do not expect higher homologs to pass through the 140 °C trap. In studying the above chemistry, and the flash pyrolysis results, at least some of the thiophene and methylthiophene observed in our pyrolysis experiments are probably results of the cracking of thiophenic precursors from the kerogen matrix. The larger quantity of methylthiophene over thiophene in our results suggests either there is less abundance of thiophene precursors in the kerogen structure, or more methylthiophene is produced because of the the lower activation energy of breaking a bond β to an aromatic system.

Acetic Acid. Figure 12 shows the acetic acid evolution profiles for all the shales except MMNG II and FSHN II (MMNG I and FSHN I, respectively, are identical), and JNUS and BROT (acetic acid evolution was not detected). The T_{max} values are also listed. The T_{max} values, in °C, for the shales not shown in the figure are: FSHN II, 426; MMNG II, 392. In general, the profiles are similar to the methylthiophene and hydrocarbon profiles except the acetic acid profiles tend to be broader, and the T_{max} values are even lower than the corresponding T_{max} values for methylthiophene. The difference between T_{max} for acetic acid evolution and T_{max} for TLO evolution was as much as 210 °C (AP24).

For the shales having fairly sharp acetic acid profiles, and T_{max} values in the range of hydrocarbon generation (FSHN, TSTB, KIMR, NAKY, and WNZN), acetic acid is probably directly related to cracking-type reactions paralleling oil formation. Barth et al.[44,45] have implicated this mechanism for acid generation from source rocks in the Kimmeridge formation. However, some of the profiles have intensity which begins in the low temperature range, well below hydrocarbon generation (WDFD, GOVT, LLNA, and AP24). This suggests an additional mechanism(s) for acetic acid generation. Immature kerogens have been treated with methanolic KOH under saponification conditions yielding acids,[46] suggesting some acetic acid may be bound by donor-acceptor interactions. This type of acid would be expected to evolve at lower temperatures than hydrocarbon evolution. In addition, Surdam et al.[47] has suggested some acids are bound to the kerogen through C-O bonds, which have lower activation energies and should therefore evolve at lower

temperatures than oil generation. This type of generation has been used to explain the production of O-containing compounds in bitumens. With the large group of shales examined, our results suggest in some cases, acetic acid generation occurs by both cracking mechanisms similar to hydrocarbon generation, and by alternative, lower energy mechanisms, as in breaking of donor-acceptor interactions. For the shales we have studied, the cracking mechanism seems to dominate, with possible minor contributions from lower energy mechanisms. AP24 is the opposite, where the lower energy mechanisms dominate the evolution. However, note even AP24 has a maximum at approximately 440 °C, indicating the cracking mechanism is also important.

Conclusions

Several important generalizations can be made from the above data:

1) Rock Eval T_{max} values and the corresponding total light organic (TLO) T_{max} values measured by TQMS have a linear relationship suggesting they can be used for similar purposes of studying pyrolysis behavior.

2) Marine shales have lower T_{max} values for TLO than lacustrine shales. This agrees well with Pyromat II and Rock Eval measurements.

3) TLO T_{max} values and the corresponding $C_4H_9^+$ T_{max} values are very similar.

4) All the shales give similar respective yields for each of the quantitated hydrocarbons -- CH_4, C_2H_6, C_2H_4, C_3H_8, and C_4H_{10}. All the shales produce about the same volume of total C_1 - C_4. The differences detected are not clearly related to kerogen source or hydrogen index.

5) Marine and lacustrine shales have different CH_4 profile shapes. For the CH_4 profile, a shoulder on the low temperature side of the prominent maximum correlates with the T_{max} values of the higher hydrocarbons for marine shales. The T_{max} values for CH_4 for lacustrine shales is very similar to the T_{max} values for the other hydrocarbons. The lacustrine shales have a shoulder on the high temperature side of the CH_4 profile that is not usually observed for the marine shales.

6) The T_{max} behavior of CH_4 generally exhibits the largest positive differences from the T_{max} for TLO, while the T_{max} values for C_4H_{10} exhibit the largest negative differences.

7) JNUS and MMNG shales are anomalies. JNUS, although terrestrial, consistently exhibits properties similar to lacustrine shales, while lacustrine MMNG exhibits properties more like marine shales.

8) CO_2 evolution is highly dependent on carbonate mineral composition. TSTB, GOVT, BROT, WNZN, AP24, and LLNA profiles are dominated by carbonate decomposition, while FSHN and MMNG profiles are dominated by siderite decomposition.

9) CO_2, CO, H_2, and H_2O show possible correlations through char gasification, and water-gas shift reactions.

10) H_2O generation is generally dominated by hydrated mineral decomposition.

11) H_2S evolution appears to be governed by FeS_2 decomposition and organo-S compound decomposition as modified by H_2S capture by iron-carbonates.

12) H_2S evolution quantitation roughly follows FeS_2 content. KIMR, NAKY, WDFD, and WNZN have high FeS_2 contents and evolve around 100 cm^3/g TOC of H_2S. PHOS, LLNA, FSHN, AP24, TSTB, MMNG, and BROT have low concentrations of pyrite and evolve less than 40 cm^3/g TOC.

13) Methylthiophene evolution follows org S/org C ratio. Marine shales have high ratios and exhibit relatively large amounts of methylthiophene. Lacustrine shales have low org S/org C ratios and evolve a relatively small amount of methylthiophene.

14) The acetic acid T_{max} value is on the leading edge of hydrocarbon generation (400-440 °C) except for AP24, which has its largest maximum at 250 °C.

Appendix

Tables A1 and A2 are included to provide a complete listing of the T_{max} values for individual hydrocarbon evolution, and total evolution (when determined) for clarity. Table A1 values are also shown in Figure 1.

Acknowledgments

We thank Jack Clarkson and Ann Murray for the Pyromat II measurements, Gordon Smith for the XRD analysis, Hugh R. Gregg, and Armando Alcaraz

for assistance with the TQMS. This work was performed under the auspices of the U. S. Department of Energy by the Lawrence Livermore National Laboratory under contract number W-7405-ENG-48.

References

1. Burnham, A. K., Braun, R. L., Gregg, H. R., and Samoun, A. M. Energy & Fuels. **1987**, 1, 452.
2. Oh, M. S., Coburn, T. T., Crawford, R. W., and Burnham, A. K. Proceedings of the International Conference on Oil Shale and Shale Oil (Chemical Industry Press, Beijing). **1988**, 295-302.
3. Wong, C. M., Crawford, R. W., and Burnham, A. K. Anal. Chem. **1984**, *56*, 390-395.
4. Oh, M. S., Taylor, R. W., Coburn, T. T., and Crawford, R. W. Energy & Fuels. **1988**, *2*(1), 100-106.
5. Coburn, T. T., Crawford, R. W., Gregg, H. R., and Oh, M. S. 1986 Eastern Oil Shale Symposium. **1987**, KECL*86-158*, 291-299.
6. Reynolds, J. G., Crawford, R. W., and Coburn, T. T. 1987 Eastern Oil Shale Symposium. **1988**, KECL*87-175*, 101-108.
7. Reynolds, J. G., and Crawford, R. W. Fuel Sci. Tech. Int'l. **1989**, *7*(5-6), 823-849.
8. Reynolds, J. G. 1988 Eastern Oil Shale Symposium. **1989**, IMMR89-201, 86-97.
9. Burnham, A. K., Oh, M. S., Crawford, R. W., and Samoun, A. M. Energy & Fuels. **1989**, *3*, 42-55.
10. Reynolds, J. G., Crawford, R. W., and Burnham, A. K. ACS Div. Fuel Chem., Preprints. **1989**, 34(4), 1106-1123.
11. Wong, C. M., Crawford, R. W., Barton, V. C., Brand, H. R., Neufeld, K. W., and Bowman, J. E. Rev. Sci. Instrum. **1983**, *54*(8), 996-1004.
12. Crawford, R. W., Brand, H. R., Wong, C. M., Gregg, H. R., Hoffman, P. A., and Enke, C. G. **1984**, *56*, 1121-1127.
13. Crawford, R. W., Alcaraz, A., and Reynolds, J. G. Anal. Chem. **1988**, 60, 2439-2441.
14. Braun, R. L., Burnham, A. K., Reynolds, J. G., and Clarkson, J. E. Energy & Fuels, accepted for publication.
15. Burnham, A. K. Energy and Fuels, accepted for publication. **1990**.
16. Espitalie, J., Ungerer, P., Irwin, I., and Marquis, F., 1988. Adv. Org. Geochem., 13 (4-6), 893-899.
17. Coburn, T. T. Energy Sources. **1983**, *7*(2), 121.
18. Huss, E. B., and Burnham, A.K. Fuel. **1982**, *61*, 1188.
19. Burnham, A. K., Huss, E. B., and Singleton, M. F. Fuel. **1983**, *62*, 1199-1204.

20 Singleton, M. F., Koskinas, G. J., Burnham, A. K., Raley, J. H. Assay Products from Green River Oil Shale. **1986**, LLNL Rept. UCRL-53273 Rev. 1.
21. Tannenbaum, E., and Kaplan, I. R. Geochim. Cosmochim. Acta. **1985**, 49, 2589-2604 .
22. Taylor, R. W., Morris, C. J., and Coburn, T. T. Proceedings 1988 Eastern Oil Shale Symposium. **1989**, IMMR88/101, 147-161 .
23. Wong, C. M., Crawford, R. W., and Burnham, A. K., ACS Div. Fuel Chem. **1984**, 29 (1), 317-321 .
24. Burnham, A. K., Stubblefield, C. T., and Campbell, J. H. Fuel. **1980**, 59, 871-877 .
25. Burnham, A. K., Clarkson, J. E., Singleton, M. F., Wong, C. M., and Crawford, R. W. Geochim. Cosmochim., Acta, **1982**, 46, 1242.
26. Coburn, T. T., Oh, M. S., Crawford, R. W., and Foster, K. G. Energy & Fuels. **1989**, 3, 216-223 .
27. Van Olphen, H., Fripiat, J. J., Eds. Data Handbook for Caly Minerals and Other Non-Metallic Minerals; Pergamon Press: Oxford, U. K. **1979**.
28. Coburn, T. T., and Barron, L. S. In Proceeding, 1984 Eastern Oil Shale Symposium. **1985**, IMMR84/124, 91-98.
29. Durand-Souron, C. Boulet, R., and Durand, B. Geochim. Cosmochim. Acta. **1982**, 46, 1193-1202.
30. Burnham, A. K., Bey, N. K., and Koskinas, G. J. ACS Symp. Ser. **1981**, 163, 61-77.
31. Burnham, A. K., and Taylor, R. W. 15th Oil shale Symp., Proceedings (Colorado School of Mines Press, Goldon, CO), 299-319.
32. Fadeff, S. K., Burnham, A. K., and Richardson, J. H., Organic and Pyritic Sulfur Determination in Oil Shale. **1983**, LLNL Report UCID-19751.
33. Reynolds J. G. unpublished results.
34. Miller, P. E., Crawford, R. W., Morris, C. J., Taylor, R. W., and Wong, C. M. 5th Briefing on Oil Shale Research. **1985**, LLNL Report MISC-4249, 375-398.
35. Oh, M. S., Burnham, A. K., and Crawford, R. W., ACS Div. Fuel Chem., Preprints. **1988**, 33(1), 274-282.
36. Attar, A. Fuel. **1978**, 57, 201-212.
37. Attar, A., Corcoran, W. H., and Gibson, G. ACS Div. Fuel Chem., Preprints. **1976**, 21(7), 106.
38. Ferm, R. J., Chem. Rev. **1957**, 57, 621-640.
39. Whelan, J., Carangelo, R. M., Soloman, P. R., and Dow, W. G. Org. Geochem., in press. **1990**.
40. Sinninghe Damste, J. S., Eglington, T. I., deLeeuw, J. W., and Schenck, P. A., Geochim. Cosmochim. Acta. **1989**, 53, 873-889 .
41. Eglinton, T. I., Sinninghe Damste, J. S., Kohnen, M. E. L., and De Leeuw, J. W. Fuel. **1990**.
42. Orr, W. L., Adv. Org. Geochem. **1986**, 10, 499-516.
43. Vallejos, C., Talukdar, S., and Philp, R. P. Energy and Fuels. **1989**, 3, 366-369 .

44. Barth, T., Borgund, A. E., Hopland, A. L., and Graue, A. Org. Geochem. **1987**, 13, 461-465 .
45. Barth, T., Borgund, E., and Hopland, A. L. Org. Geochem., **1989**, 14, 69-76 .
46. Kawamura, K., and Ishiwatari, R. Org. Geochem. **1985**, 8, 197-202 .
47. Surdam, R. C., Boese, S. W., and Crossey, L. J., AAPG Memoir 37: Clastic Diagenesis (Ed McDonald, D. A., and Surdam, R. C.), **1984**, 127-150 .

Table 1.

Pyrolysis Products Monitored by TQMS (Species and m/z)

Hydrocarbons		O and N Compounds		S Compounds	
H_2	2	H_2O	18	H_2S	34/32
CH_4	16, 16/14	CO	28/84	CH_3SH	48/45
C_2H_4	26, 28/26	CH_3CO	43/16	COS	60/32
C_2H_6	30, 30/27	CO_2	44/16	C_2H_5SH	62/29
C_3H_6	42, 42/39	CH_3COOH	60/45	CH_3SCH_3	62/47
C_3H_8	44/29	C_4H_5N	67/40	SO_2	64/48
C_4H_8	56	C_5H_5N	79/52	CS_2	76/32
C_4H_{10}	58	C_6H_5OH	94/65	C_3H_7SH	76/42
C_5H_{10}	70			C_4H_4S	84/45
C_5H_{12}	72			$CH_3C_4H_4S$	97/53
C_6H_6	78/52				
C_6H_{12}	84/56				
C_6H_{14}	86				
$CH_3C_6H_5$	92/91				
C_7H_{10}	94/79				

Table 2. Oil Shale Descriptions

Shale	Country	Type	Minerals	Clay/Quartz
JNUS	Norway	Terestrial	Quartz, Illite (m), Kaolinite (tr), Pyrite (tr)	0.78
KIMR	North Sea	Marine	Quartz, Illite, Pyrite (m), Feldspar (tr), Dolomite (tr), Kaolinite (tr)	0.36
PHOS	Montana	Marine	Quartz, Illite (m), Siderite (tr), Pyrite (tr), Kaolinite (tr)	0.45
NAKY	Kentucky	Marine	Quartz, Illite (m), Kaolinite (tr), Feldspar (tr), Pyrite (tr)	0.27
WDFD	Oklahoma	Marine	Quartz, Pyrite (tr), Kaolinite (tr), Illite (tr), Smectite (tr)	0.46
LLNA	Venezuela	Marine	Calcite, Quartz, Kaolinite (tr)	0.05
WNZN	West Germany	Marine	Calcite, Quartz, Kaolinite (m), Illite (tr), Pyrite (tr)	0.10
TSTB	Norway	Marine	Quartz, Siderite (m), Calcite (m), Pyrite (m), Illite (m), Kaolinite (m)	0.37
MMNG I	China	Lacustrine	Quartz, Kaolinite, Siderite (tr), Illite (tr)	0.82
MMNG II	China	Lacustrine	Quartz, Kaolinite, Siderite (m), Illite (tr)	0.84
FSHN I	China	Lacustrine	Quartz, Kaolinite, Siderite (m), {Halite}, Illite (tr), Smectite (tr)	0.60
FSHN II	China	Lacustrine	Quartz, Kaolinite, Siderite (m), {Halite}	0.50
AP24	Colorado	Lacustrine	Dolomite, Quartz, Calcite (m), Feldspar (m), Analcime (m), Pyrite (tr), Illite(tr)	0.15
GOVT	Utah	Lacustrine	Quartz, Dolomite (m), Calcite (m), Illite (m), Analcime (tr), Kaolinite (tr)	0.38
BROT	Utah	Lacustrine	Dolomite, Quartz, Calcite, Feldspar (m), Smectite (m), Analcime (tr), Illite (tr)	0.36

Minerals in {} are tentative
(m) = minor components
(tr) = trace components

Table 3. Chemical Analysis of Selected Oil Shales, % by Weight of Total Sample

	oil[b]	tot C	tot H	tot N	acid CO_2	org C	tot S	SO_4	FeS	FeS_2	org S	org S/org C[a]
JNUS	-.-	1.9	0.9	0.1	1.2	1.6	1.5	0.1	0.1	1.1	0.1	0.023
KIMR	2.0	6.4	1.5	0.4	0.8	6.2	3.3	0.7	0.0	2.3	0.3	0.021
PHOS	5.2	16.8	2.2	0.8	0.5	16.6	1.8	0.1	0.2	0.5	1.0	0.023
NAKY	4.3	11.4	1.4	0.2	1.0	11.1	4.4	0.0	0.2	3.8	0.5	0.016
WDFD	5.0	15.6	1.6	0.7	0.8	15.4	3.3	0.2	0.1	2.2	0.8	0.019
LLNA	4.6	17.8	1.3	0.4	24.4	11.2	1.4	0.0	0.1	0.4	0.9	0.031
WNZN	5.6	16.3	1.6	0.3	17.2	11.6	3.0	0.3	0.1	2.0	0.7	0.022
TSTB	-.-	8.2	1.2	0.3	4.3	6.9	1.3	0.1	0.2	0.8	0.3	0.014
MMNG I	-.-	14.8	2.8	0.6	1.7	14.3	1.4	na	na	na	na	na
MMNG II	5.0	18.1	2.7	0.8	3.8	17.0	1.7	0.2	0.4	0.9	0.3	0.006
FSHN I	-.-	11.8	2.4	0.7	3.8	10.8	0.6	na	na	na	na	na
FSHN II	5.9	11.9	2.0	0.8	3.3	11.0	0.7	0.0	0.0	0.5	0.2	0.008
AP24	9.0	15.6	1.6	0.5	17.1	9.9	0.7	0.0	0.1	0.4	0.2	0.006
GOVT	4.1	9.2	1.3	0.5	9.9	6.5	0.7	0.1	0.0	0.5	0.1	0.006
BROT	2.9	9.7	0.8	0.3	19.1	4.4	0.2	0.0	0.0	0.2	0.0	0.004

[a] Atomic ratio calculated before rounding.

[b] Oil produced at 2°C/min heating rate, autogenous flow.

Table 4.

Temperatures of Maximum Evolution (T_{max}) for Total Light Organics (TLO), $C_4H_9^+$ Ions from Hydrocarbons, Total Pyrolysate from Pyromat II Micropyrolyzer, and Standard Rock Eval Pyrolysis

Shale	TLO, °C[a]	$C_4H_9^+$, °C[a]	Pyromat II, °C[b]	Rock Eval, °C[c]
JNUS	460	462	463	438
KIMR	445	450	442	426
PHOS	447	446	441	425
NAKY	442	442	443	425
WDFD	447	453	444	426
LLNA	449	449	444	428
WNZN	450	455	444	426
TSTB	458	458	456	432
MMNG I	457	457	452	na
MMNG II	458	455	451	435
FSHN I	457	460	459	na
FSHN II	455	456	462	440
AP24	466	466	459	443
GOVT	463	459	452	433
BROT	472	472	467	448

na = not available

a. heating rate, 10 °C/min

b. heating rate, 9.2 °C/min

c. heating rate, 25-30 °C/min

Table 5. CO_2 Balance for Shales

Shale	CO_2 cc/g shale[a]	CO cc/g shale[a]	CO_2 by acid carbonate[c]	CO_2 by TQMS[b,c]
JNUS	7.7	2.6	1.2	1.5
KIMR	8.7	4.7	0.8	1.8
PHOS	13.3	19.8	0.5	3.5
NAKY	8.0	6.7	1.0	1.8
WDFD	13.2	4.6	0.8	2.6
LLNA	80.1	121.7	24.1	21.2
WNZN	87.5	79.3	17.2	20.1
TSTB	19.9	16.2	4.3	4.5
MMNG II	16.1	8.2	3.8	3.3
FSHN I	23.0	10.6	3.3	4.7
AP24	81.1	45.2	17.2	17.1
GOVT	72.5	34.0	14.9	9.9
BROT	116.2	47.5	19.1	23.5

a. Corrected for STP

b. $CO_2 total = CO_{2 measured} + (1/2)CO_{measured}$

c. Weight percent of shale.

Table 6.

COS Evolution for Selected Oil Shales at the Heating Rate of 10°C/min

Shale	Peak 1, °C (%)	Peak 2, °C (%)	Peak 3, °C (%)
JNUS	nd	534 (53)	809 (47)
KIMR	406 (15)	554 (34)	809 (52)
PHOS	335 (100)	nd	nd
NAKY	400 (12)	530 (51)	817 (38)
WDFD	346 (59)	527 (41)	nd
LLNA	370 (16)	nd	809 (84)
WNZN	400 (9)	534 (18)	759 (73)
TSTB	nd	nd	nd
MMNG I	393 (100)	nd	nd
MMNG II	379 (100)	nd	nd
FSHN I	404 (100)	nd	nd
FSHN II	402 (100)	nd	nd
AP24	389 (XX)	nd	799 (YY)
GOVT	445 (12)	544 (19)	793 (69)
BROT	nd	nd	790 (100)

nd not detected

a. (%) = percent of total profile

Table 7.

Thiophene and Methylthiophene Evolution for Selected Oil Shales at the Heating Rate of 10°C/min

Oil Shale	Thiophene		Methylthiophene	
	T_{max}, °C	cm^3/g of TOC[a]	T_{max}	cm^3/g of TOC[a]
KIMR	426	0.35	417	0.94
PHOS	420	0.14	430	0.98
NAKY	431	0.02	431	0.09
WDFD	421	0.12	428	0.51
LLNA	428	0.13	437	0.97
WNZN	425	0.09	435	0.72
TSTB	433	0.01	441	0.23
MMNG I	{450}	{0.01}	437	0.09
MMNG II	{421}	{0.01}	423	0.09
FSHN I	429	0.01	430	0.16
FSHN II	431	0.03	430	0.21
AP24	441		441	
GOVT	430	0.03	449	0.12
BROT	nd	-	462	0.05

{} indicates extremely low intensity, data marginal at best.
nd not detected.
a. TOC = total organic carbon

Table A1. Summary of T_{max} and Total Evolution Data for CH_4, C_2H_6, C_2H_4, C_3H_8, and C_4H_{10} for Selected Shales at the Heating Rate of 10 °C/min.

	CH_4		C_2H_6		C_2H_4		C_3H_8		C_4H_{10}	
Shale	T_{max}, °C	Total Evol., cm^3/g TOC	T_{max}, °C	Total Evol., cm^3/g TOC	T_{max}, °C	Total Evol., cm^3/g TOC	T_{max}, °C	Total Evol., cm^3/g TOC	T_{max}, °C	Total Evol., cm^3/g TOC
JNUS	500	49.1	463	14.0	464	4.6	464	8.1	460	3.5
KIMR	482	30.1	460	4.8	471	3.5	449	2.4	432	5.4
PHOS	502	62.2	456	11.7	472	7.5	438	6.3	431	7.4
NAKY	495	60.6	453	13.7	475	8.7	441	6.1	432	6.7
WDFD	513	48.5	459	14.8	479	4.2	446	13.3	429	5.9
LLNA	506	55.7	457	11.8	465	6.2	455	2.8	442	6.1
WNZN	497	38.4	455	10.5	480	4.0	453	4.0	440	11.2
TSTB	495	47.0	466	15.4	483	5.9	457	3.5	454	5.9
MMNG I	492	30.5	464	8.2	491	2.8	460	3.1	443	5.5
MMNG II	482	30.5	461	7.1	479	2.8	451	2.3	439	5.1
FSHN I	471	40.0	457	18.0	460	4.8	455	3.7	446	8.3
FSHN II	463	41.1	453	9.8	456	3.3	455	3.4	443	6.0
AP24	469	34.4	468	12.4	471	4.0	468	5.4	463	18.4
GOVT	485	82.5	463	12.3	469	2.3	458	12.7	459	6.6
BROT	479	27.1	472	8.9	474	8.9	473	3.4	472	5.0

Table A2. Temperature of Maximum Evolution (°C) for Higher Hydrocarbons for Selected Oil Shales at a Heating Rate of 10 °C/min.

Oil Shale	C_5H_{10}	C_5H_{12}	C_6H_6	C_6H_{12}	C_7H_8	C_7H_{10}
JNUS	455 (240)	463	453	456	461	456
KIMR	450 (177)	440 (211)	431	458	436	426
PHOS	446	441	455	455	450	445
NAKY	442 (175)	435	435	438 (200)	442	435
WDFD	447 (200)	440	435	447	nd	432
LLNA	449	446	447	447	449	440
WNZN	460	450	444	454	455	449
TSTB	462 (155)	459 (200)	451	461 (181)	nd	458
MMNG I	457	451	457	464	461	457
MMNG II	461	451	457	469	451	449
FSHN I	457 (271)	450 (267)	449 (288)	456	456	453
FSHN II	456 (168)	453	455	461	462	453
AP24	466	466	475	469	472	466
GOVT	468 (160)	473	473	479	479	453
BROT	472	464	472	471	nd	479

nd. not detected

values in parenthesis are T_{max} values for low temperature maximum assigned to entrapped hydrocarbons.

Figures

Figure 1. Evolution of CH_4, C_2H_6, C_2H_4, C_3H_8, and C_4H_{10} as a function of pyrolysis temperature for selected oil shales at the heating rate of 10°C/min. T_{max} values (arrows), shoulder T_{max} values (dotted arrows) and total evolutions in cm^3/g TOC are also given.

Figure 2. Differences of T_{max} Values for selected species measured by the TQMS as related to corresponding rock eval T_{max} values.

Figure 3. Differences of the T_{max} Values for TLO and T_{max} values for individual hydrocarbons for selected hydrocarbons measured by the TQMS. Y-Axis divisions are 12.5 °C.

Figure 4. Carbon dioxide evolution as a function of pyrolysis temperature for A) high carbonate shales, B) low carbonate shales, C) siderite shales, and D) 300 to 600 °C temperature range for all the shales at the heating rate of 10°C/min. The profiles are normalized for ease of display. Total evolution, in cm^3/g of shale, is indicated for each shale in parentheses.

Figure 5. Carbon monoxide evolution as a function of pyrolysis temperature for selected oil shales at the heating rate of 10°C/min. The profiles are normalized for ease of display. Total evolution, in cm^3/g of shale, is indicated for each shale in parentheses.

Figure 6. Comparison of CO and CO_2 evolution profiles evolution as a function of pyrolysis temperature for A) GOVT, and B) NAKY shales at the heating rate of 10°C/min. The profiles are normalized for ease of display.

Figure 7. Hydrogen evolution as a function of pyrolysis temperature for selected oil shales at the heating rate of 10°C/min. Y-Axis divisions are 10 cm^3/min-g TOC. Total evolution is indicated in parentheses for each shale. T_{max} values are for maximum assigned to hydrocarbon evolution and percentage of total evolution is indicated.

Figure 8. Water evolution as a function of pyrolysis temperature for selected oil shales at the heating rate of 10°C/min. Profiles are normalized for ease of display. Total evolution in cm^3/g of shale is indicated for each shale in parentheses.

Figure 9. Hydrogen sulfide evolution as a function of pyrolysis temperature for (see text) A) Category 1 Shales, B) Category 2 Shales, and 3) Category 3 shales at the heating rate of 10°C/min. Profiles are normalized for ease of display. Total evolution, in cm^3/g of TOC, is indicated for each shale in parentheses.

Figure 10. Methylthiophene evolution as a function of pyrolysis temperature for selected oil shales at the heating rate of 10°C/min. Profiles are normalized for ease of display.

Figure 11. Total methylthiophene evolution (Measured by TQMS) as a function of Org S/Org C in selected shales.

Figure 12. Acetic acid evolution as a function of pyrolysis temperature for selected oil shales at the heating rate of 10°C/min. Profiles are normalized for ease of display. PHOS (omitted for clarity) has T_{max} of 414 °C.

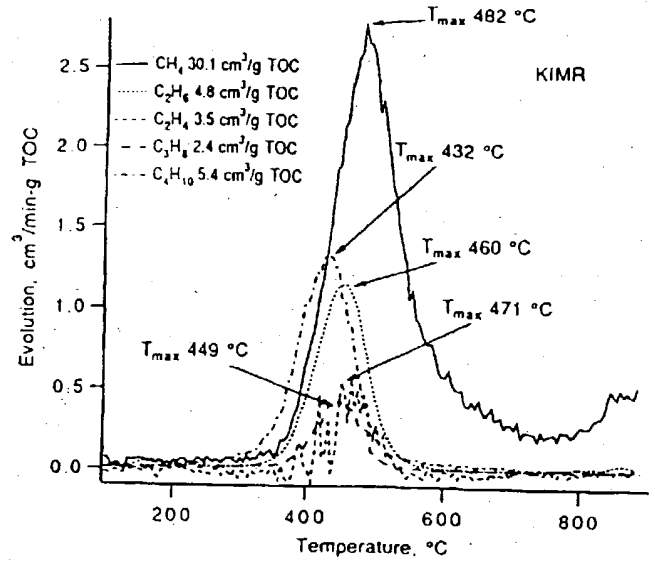
KIMR
CH_4 30.1 cm³/g TOC
C_2H_6 4.8 cm³/g TOC
C_2H_4 3.5 cm³/g TOC
C_3H_8 2.4 cm³/g TOC
C_4H_{10} 5.4 cm³/g TOC
T_{max} 482 °C
T_{max} 432 °C
T_{max} 460 °C
T_{max} 471 °C
T_{max} 449 °C
Evolution, cm³/min-g TOC
Temperature, °C

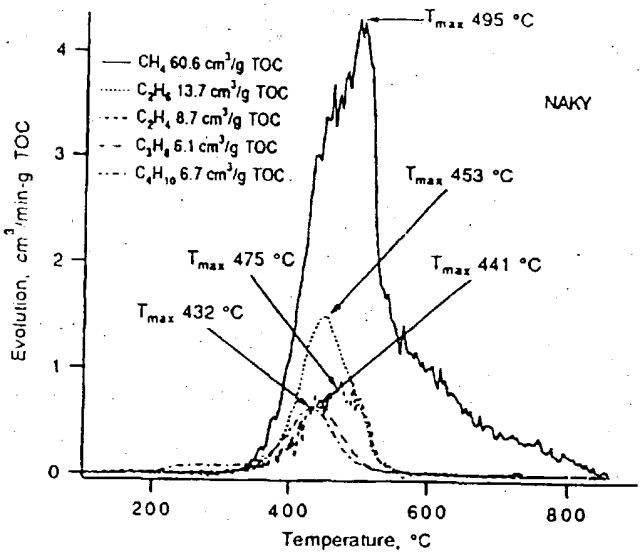
NAKY
CH_4 60.6 cm³/g TOC
C_2H_6 13.7 cm³/g TOC
C_2H_4 8.7 cm³/g TOC
C_3H_8 6.1 cm³/g TOC
C_4H_{10} 6.7 cm³/g TOC
T_{max} 495 °C
T_{max} 453 °C
T_{max} 475 °C
T_{max} 441 °C
T_{max} 432 °C
Evolution, cm³/min-g TOC
Temperature, °C

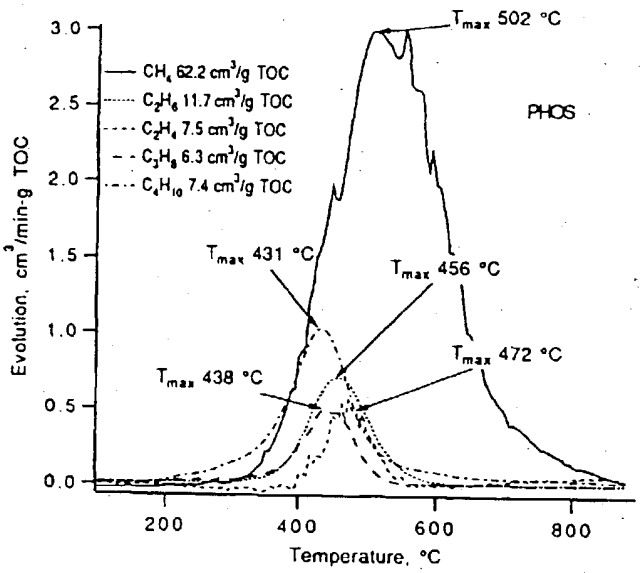
PHOS
CH_4 62.2 cm³/g TOC
C_2H_6 11.7 cm³/g TOC
C_2H_4 7.5 cm³/g TOC
C_3H_8 6.3 cm³/g TOC
C_4H_{10} 7.4 cm³/g TOC
T_{max} 502 °C
T_{max} 431 °C
T_{max} 456 °C
T_{max} 472 °C
T_{max} 438 °C
Evolution, cm³/min-g TOC
Temperature, °C

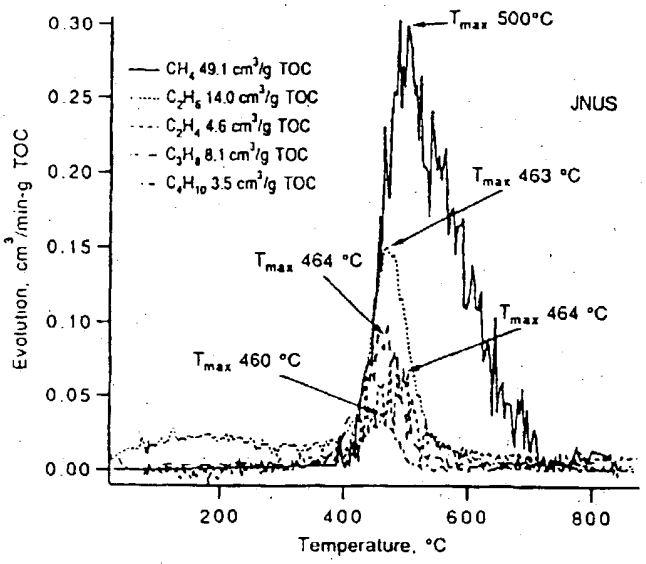
JNUS
CH_4 49.1 cm³/g TOC
C_2H_6 14.0 cm³/g TOC
C_2H_4 4.6 cm³/g TOC
C_3H_8 8.1 cm³/g TOC
C_4H_{10} 3.5 cm³/g TOC
T_{max} 500°C
T_{max} 463 °C
T_{max} 464 °C
T_{max} 464 °C
T_{max} 460 °C
Evolution, cm³/min-g TOC
Temperature, °C

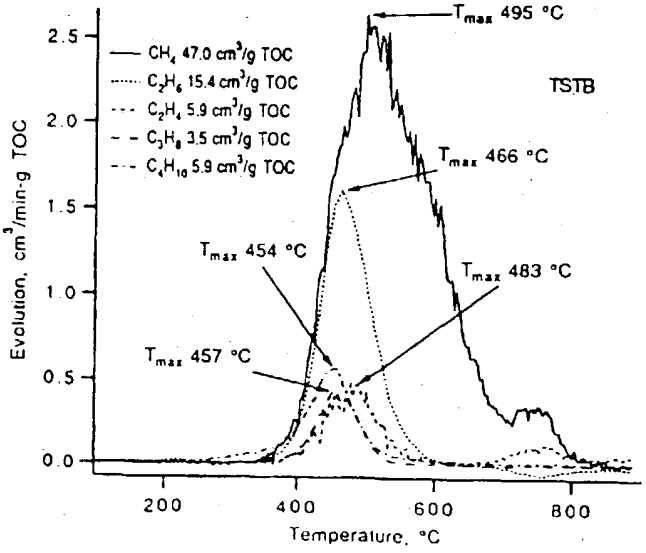
TSTB
CH_4 47.0 cm³/g TOC
C_2H_6 15.4 cm³/g TOC
C_2H_4 5.9 cm³/g TOC
C_3H_8 3.5 cm³/g TOC
C_4H_{10} 5.9 cm³/g TOC
T_{max} 495 °C
T_{max} 466 °C
T_{max} 454 °C
T_{max} 483 °C
T_{max} 457 °C
Evolution, cm³/min-g TOC
Temperature, °C

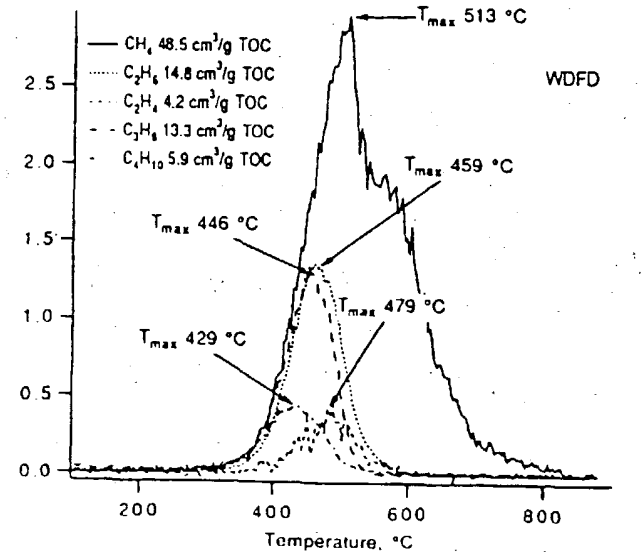
WDFD
CH_4 48.5 cm³/g TOC
C_2H_6 14.8 cm³/g TOC
C_2H_4 4.2 cm³/g TOC
C_3H_8 13.3 cm³/g TOC
C_4H_{10} 5.9 cm³/g TOC
T_{max} 513 °C
T_{max} 459 °C
T_{max} 446 °C
T_{max} 479 °C
T_{max} 429 °C
Evolution, cm³/min-g TOC
Temperature, °C

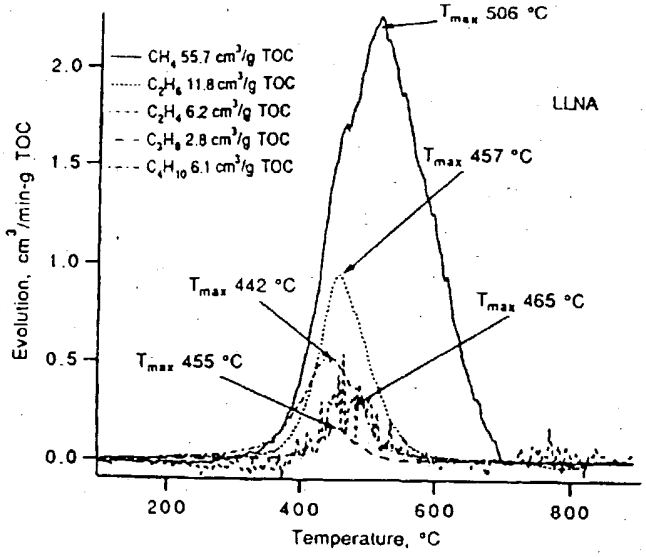
LLNA
CH_4 55.7 cm³/g TOC
C_2H_6 11.8 cm³/g TOC
C_2H_4 6.2 cm³/g TOC
C_3H_8 2.8 cm³/g TOC
C_4H_{10} 6.1 cm³/g TOC
T_{max} 506 °C
T_{max} 457 °C
T_{max} 442 °C
T_{max} 465 °C
T_{max} 455 °C
Evolution, cm³/min-g TOC
Temperature, °C

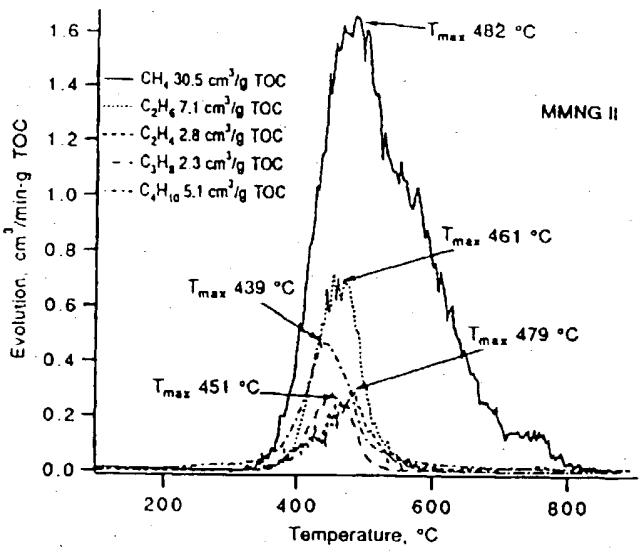
MMNG II
CH_4 30.5 cm³/g TOC
C_2H_6 7.1 cm³/g TOC
C_2H_4 2.8 cm³/g TOC
C_3H_8 2.3 cm³/g TOC
C_4H_{10} 5.1 cm³/g TOC
T_{max} 482 °C
T_{max} 461 °C
T_{max} 439 °C
T_{max} 479 °C
T_{max} 451 °C
Evolution, cm³/min-g TOC
Temperature, °C

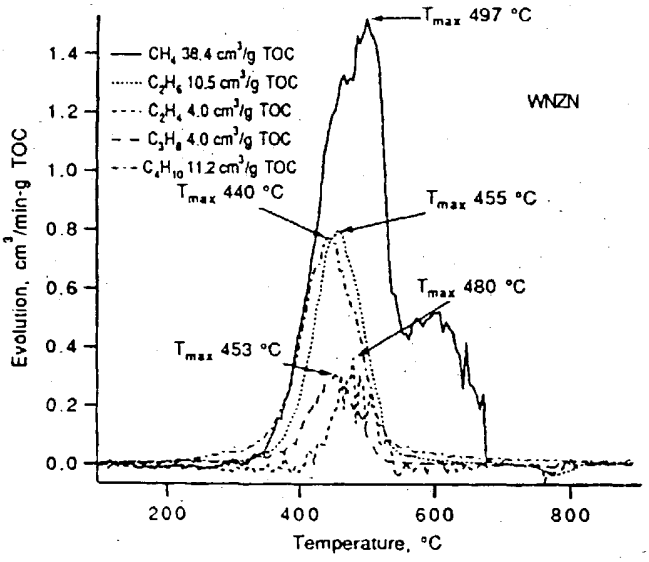
WNZN
CH_4 38.4 cm³/g TOC
C_2H_6 10.5 cm³/g TOC
C_2H_4 4.0 cm³/g TOC
C_3H_8 4.0 cm³/g TOC
C_4H_{10} 11.2 cm³/g TOC
T_{max} 497 °C
T_{max} 440 °C
T_{max} 455 °C
T_{max} 480 °C
T_{max} 453 °C
Evolution, cm³/min-g TOC
Temperature, °C

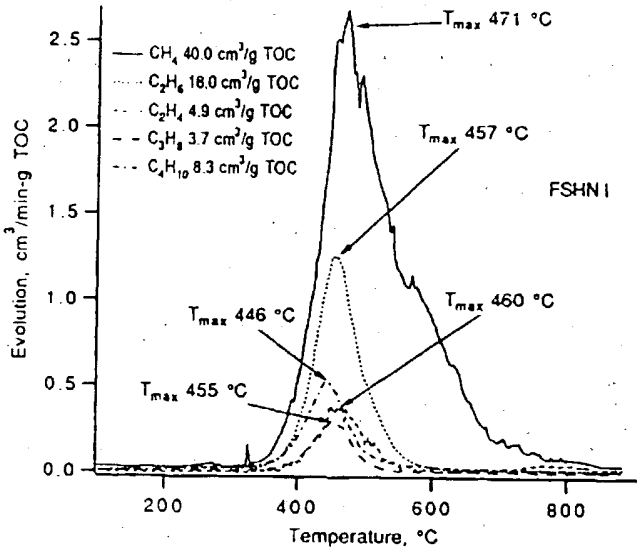
FSHN I
CH_4 40.0 cm³/g TOC
C_2H_6 18.0 cm³/g TOC
C_2H_4 4.9 cm³/g TOC
C_3H_8 3.7 cm³/g TOC
C_4H_{10} 8.3 cm³/g TOC
T_{max} 471 °C
T_{max} 457 °C
T_{max} 446 °C
T_{max} 460 °C
T_{max} 455 °C
Evolution, cm³/min-g TOC
Temperature, °C

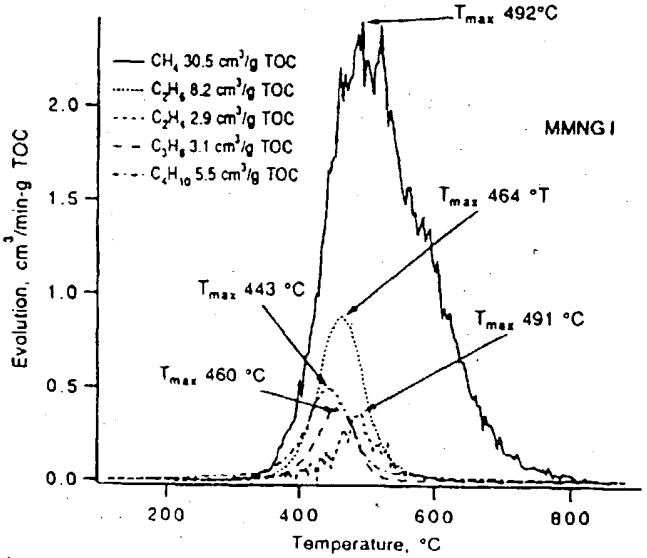
MMNG I
CH_4 30.5 cm³/g TOC
C_2H_6 8.2 cm³/g TOC
C_2H_4 2.9 cm³/g TOC
C_3H_8 3.1 cm³/g TOC
C_4H_{10} 5.5 cm³/g TOC
T_{max} 492°C
T_{max} 464 °T
T_{max} 443 °C
T_{max} 491 °C
T_{max} 460 °C
Evolution, cm³/min-g TOC
Temperature, °C

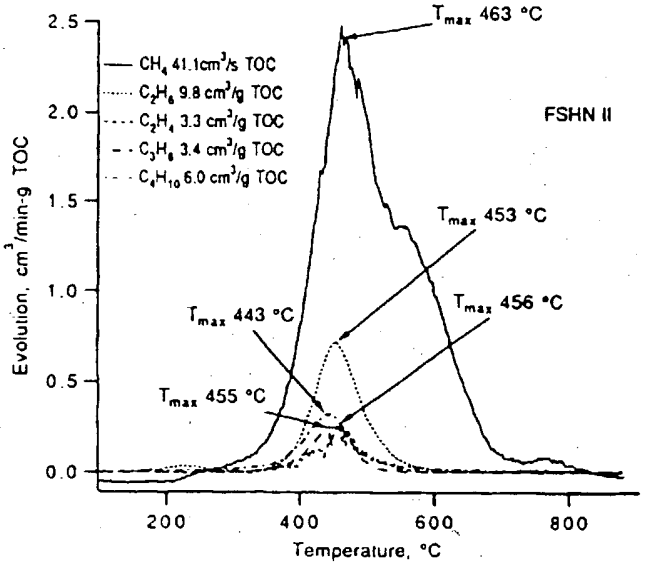
FSHN II
CH_4 41.1cm³/s TOC
C_2H_6 9.8 cm³/g TOC
C_2H_4 3.3 cm³/g TOC
C_3H_8 3.4 cm³/g TOC
C_4H_{10} 6.0 cm³/g TOC
T_{max} 463 °C
T_{max} 453 °C
T_{max} 443 °C
T_{max} 456 °C
T_{max} 455 °C
Evolution, cm³/min-g TOC
Temperature, °C

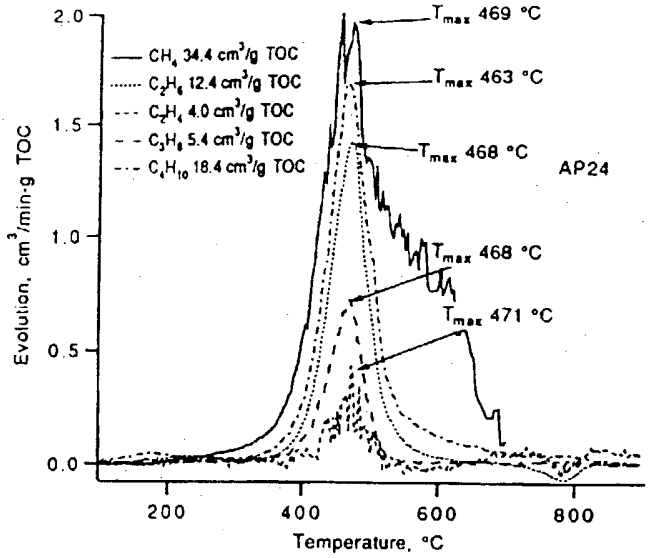
CH_4 34.4 cm³/g TOC
C_2H_6 12.4 cm³/g TOC
C_2H_4 4.0 cm³/g TOC
C_3H_8 5.4 cm³/g TOC
C_4H_{10} 18.4 cm³/g TOC
T_{max} 469 °C
T_{max} 463 °C
T_{max} 468 °C
AP24
T_{max} 468 °C
T_{max} 471 °C
Evolution, cm³/min-g TOC
Temperature, °C

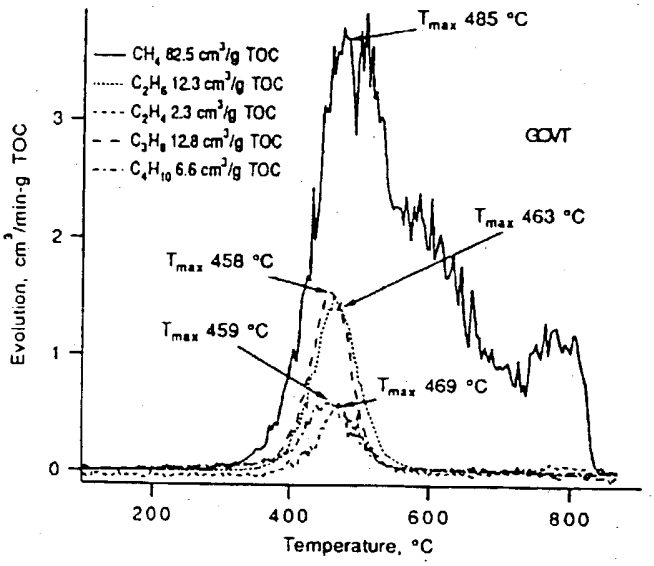
CH_4 82.5 cm³/g TOC
C_2H_6 12.3 cm³/g TOC
C_2H_4 2.3 cm³/g TOC
C_3H_8 12.8 cm³/g TOC
C_4H_{10} 6.6 cm³/g TOC
T_{max} 485 °C
GCVT
T_{max} 463 °C
T_{max} 458 °C
T_{max} 459 °C
T_{max} 469 °C
Evolution, cm³/min-g TOC
Temperature, °C

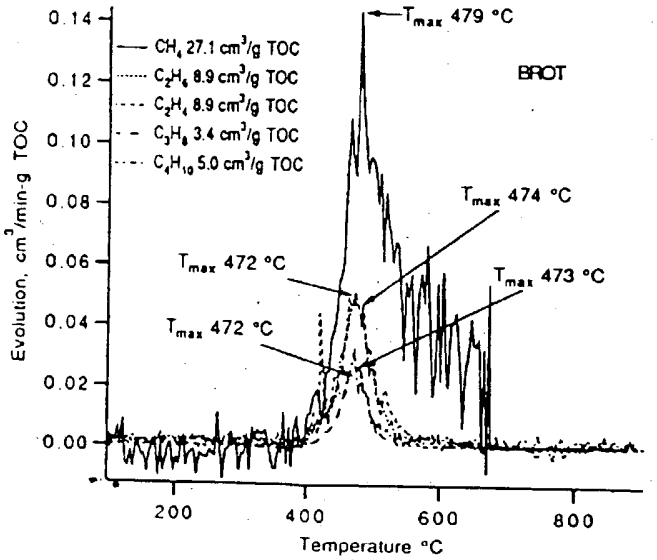
CH_4 27.1 cm³/g TOC
C_2H_6 8.9 cm³/g TOC
C_2H_4 8.9 cm³/g TOC
C_3H_8 3.4 cm³/g TOC
C_4H_{10} 5.0 cm³/g TOC
T_{max} 479 °C
BROT
T_{max} 474 °C
T_{max} 472 °C
T_{max} 473 °C
T_{max} 472 °C
Evolution, cm³/min-g TOC
Temperature °C

Figure 2

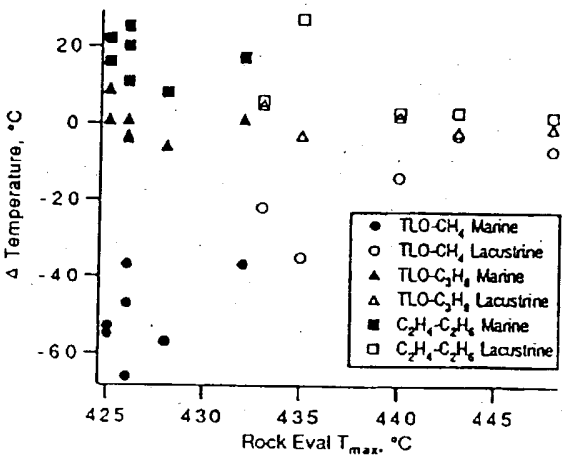
20
0
-20
-40
-60
Δ Temperature, °C
425
430
435
440
445
Rock Eval T_{max}, °C
TLO-CH_4 Marine
TLO-CH_4 Lacustrine
TLO-C_2H_6 Marine
TLO-C_2H_6 Lacustrine
C_2H_4-C_2H_6 Marine
C_2H_4-C_2H_6 Lacustrine

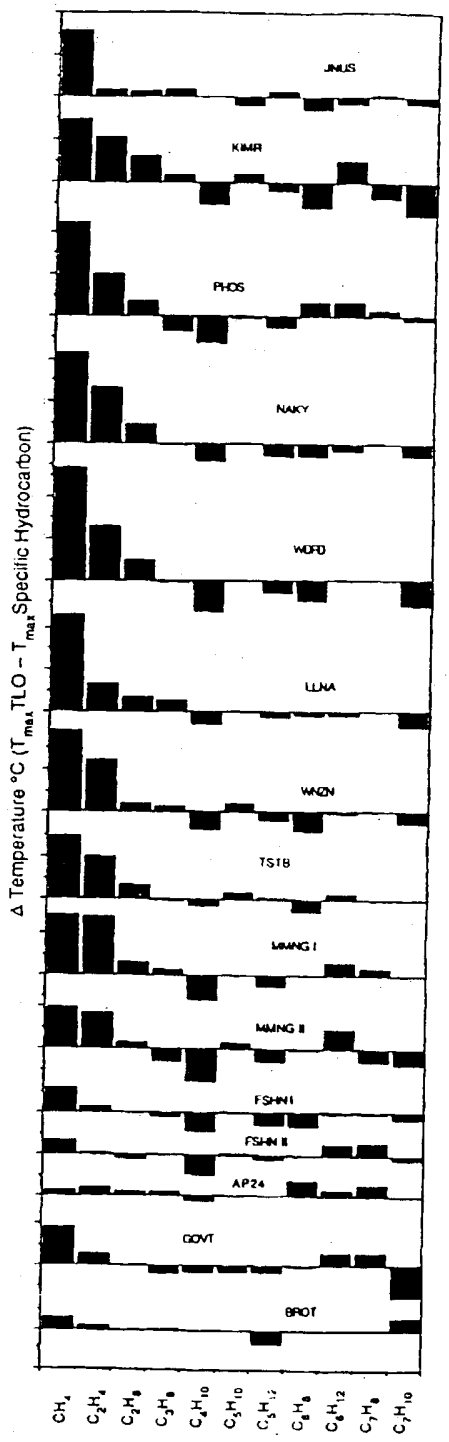
Δ Temperature °C (T_{max}TLO – T_{max} Specific Hydrocarbon)
JINJIS
KIMR
PHOS
NAKY
WDFD
LUNA
WAZN
TSTB
MMNG I
MMNG II
FSHN I
FSHN II
AP24
GOVT
BROT
CH_4
C_2H_4
C_2H_6
C_3H_8
C_4H_{10}
C_5H_{10}
C_5H_{12}
C_6H_6
C_6H_{12}
C_7H_8
C_7H_{16}

Figure 4

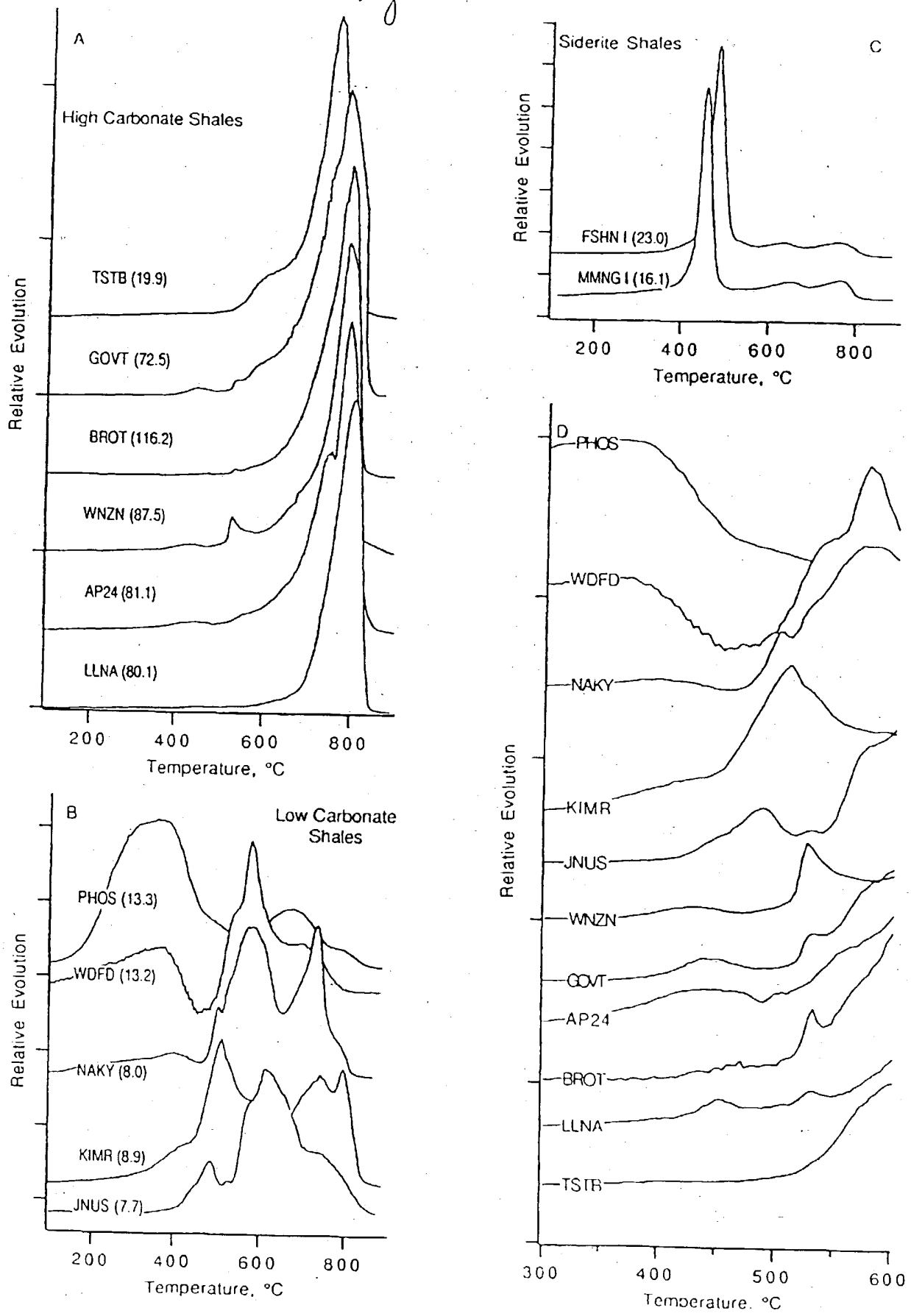
A
High Carbonate Shales
TSTB (19.9)
GOVT (72.5)
BROT (116.2)
WNZN (87.5)
AP24 (81.1)
LLNA (80.1)
Relative Evolution
200
400
600
800
Temperature, °C
B
Low Carbonate Shales
PHOS (13.3)
WDFD (13.2)
NAKY (8.0)
KIMR (8.9)
JNUS (7.7)
Relative Evolution
200
400
600
800
Temperature, °C
Siderite Shales
C
FSHN I (23.0)
MMNG I (16.1)
Relative Evolution
200
400
600
800
Temperature, °C
D
PHOS
WDFD
NAKY
KIMR
JNUS
WNZN
GOVT
AP24
BROT
LLNA
TSTB
Relative Evolution
300
400
500
600
Temperature, °C

Figure 5

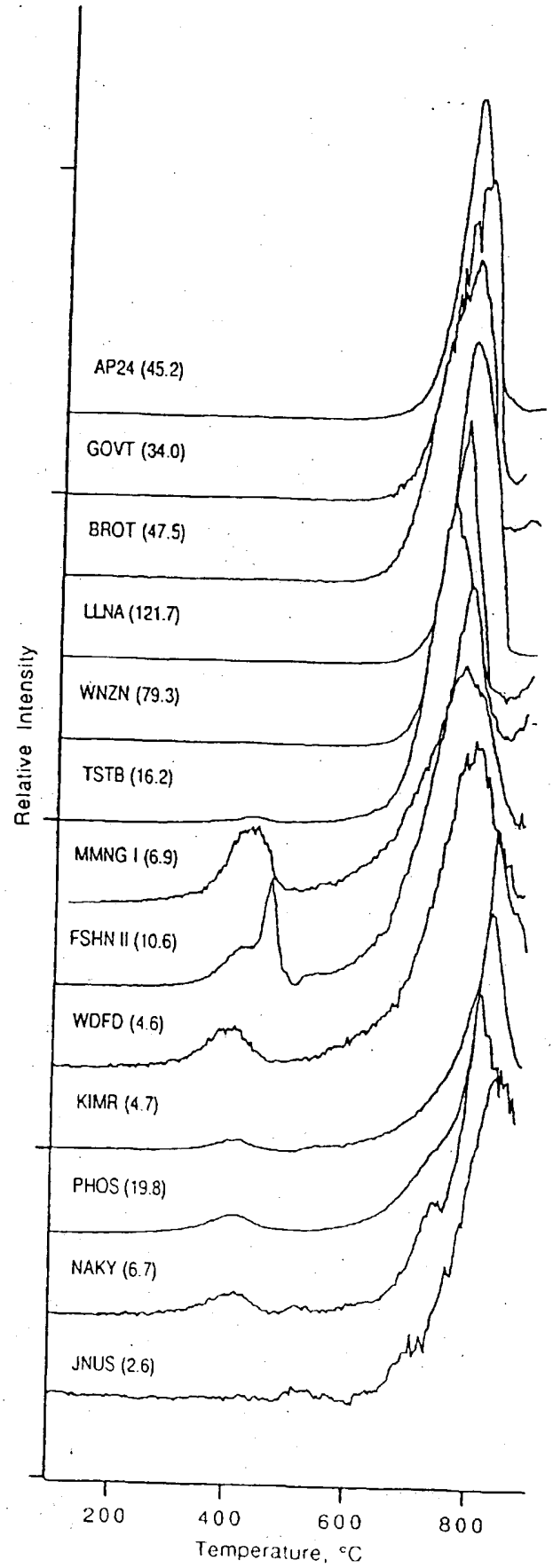
AP24 (45.2)
GOVT (34.0)
BROT (47.5)
LLNA (121.7)
WNZN (79.3)
TSTB (16.2)
MMNG I (6.9)
FSHN II (10.6)
WDFD (4.6)
KIMR (4.7)
PHOS (19.8)
NAKY (6.7)
JNUS (2.6)
Relative Intensity
200
400
600
800
Temperature, °C

Figure 6

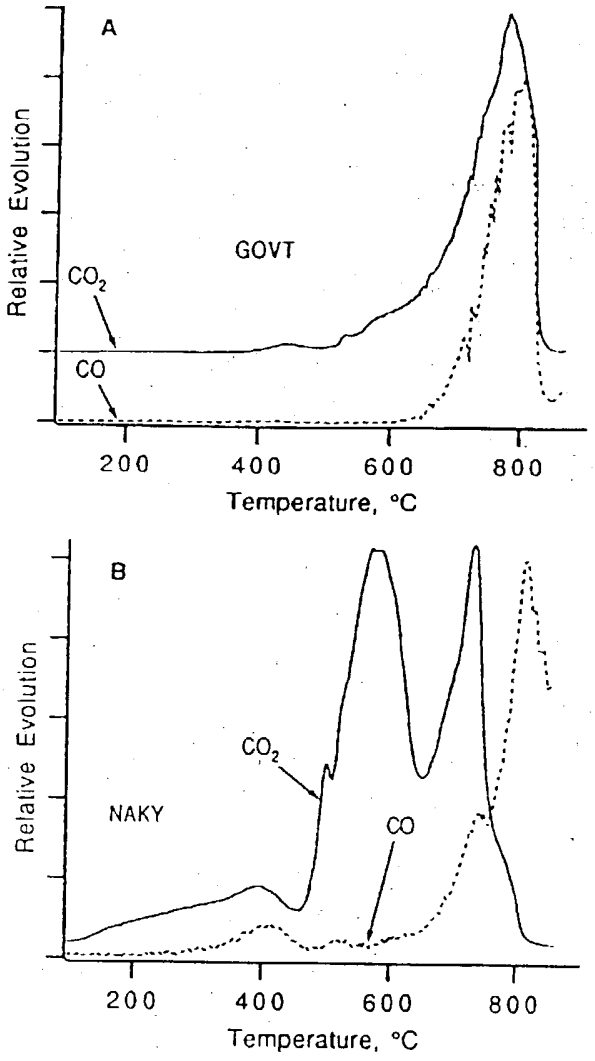
A
Relative Evolution
GOVT
CO_2
CO
200
400
600
800
Temperature, °C
B
Relative Evolution
NAKY
CO_2
CO
200
400
600
800
Temperature, °C

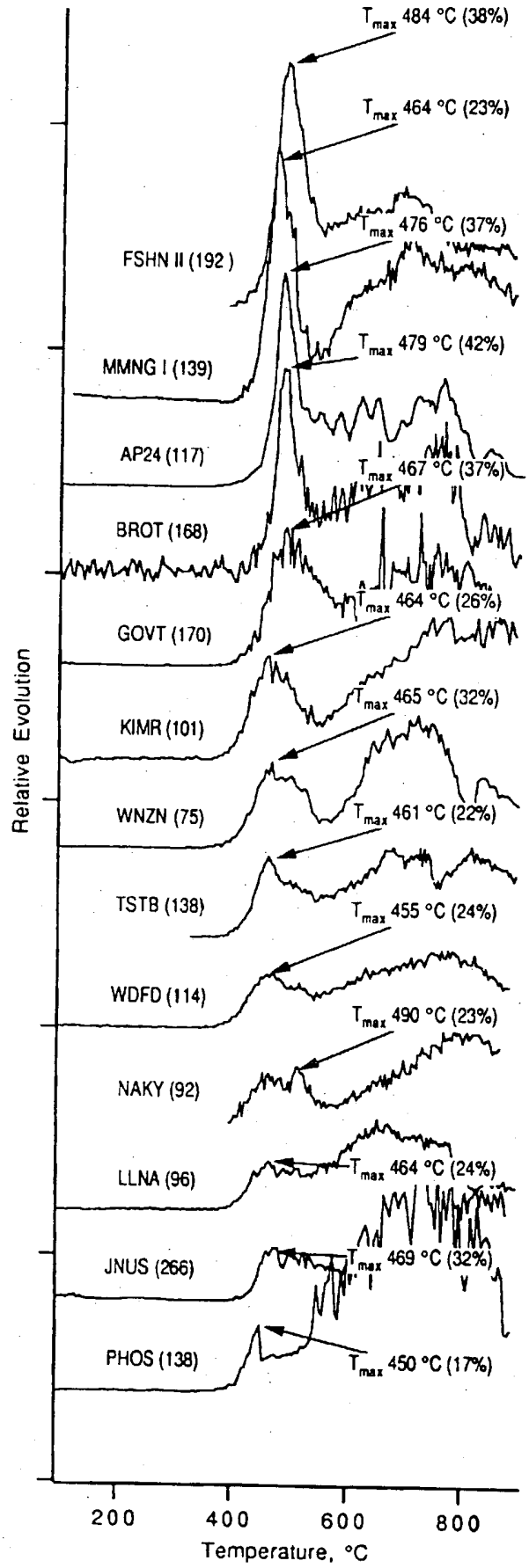
T_{max} 484 °C (38%)
T_{max} 464 °C (23%)
T_{max} 476 °C (37%)
FSHN II (192)
T_{max} 479 °C (42%)
MMNG I (139)
AP24 (117)
T_{max} 467 °C (37%)
BROT (168)
T_{max} 464 °C (26%)
GOVT (170)
T_{max} 465 °C (32%)
KIMR (101)
T_{max} 461 °C (22%)
WNZN (75)
T_{max} 455 °C (24%)
TSTB (138)
T_{max} 490 °C (23%)
WDFD (114)
T_{max} 464 °C (24%)
NAKY (92)
T_{max} 469 °C (32%)
LLNA (96)
T_{max} 450 °C (17%)
JNUS (266)
PHOS (138)
Relative Evolution
200
400
600
800
Temperature, °C

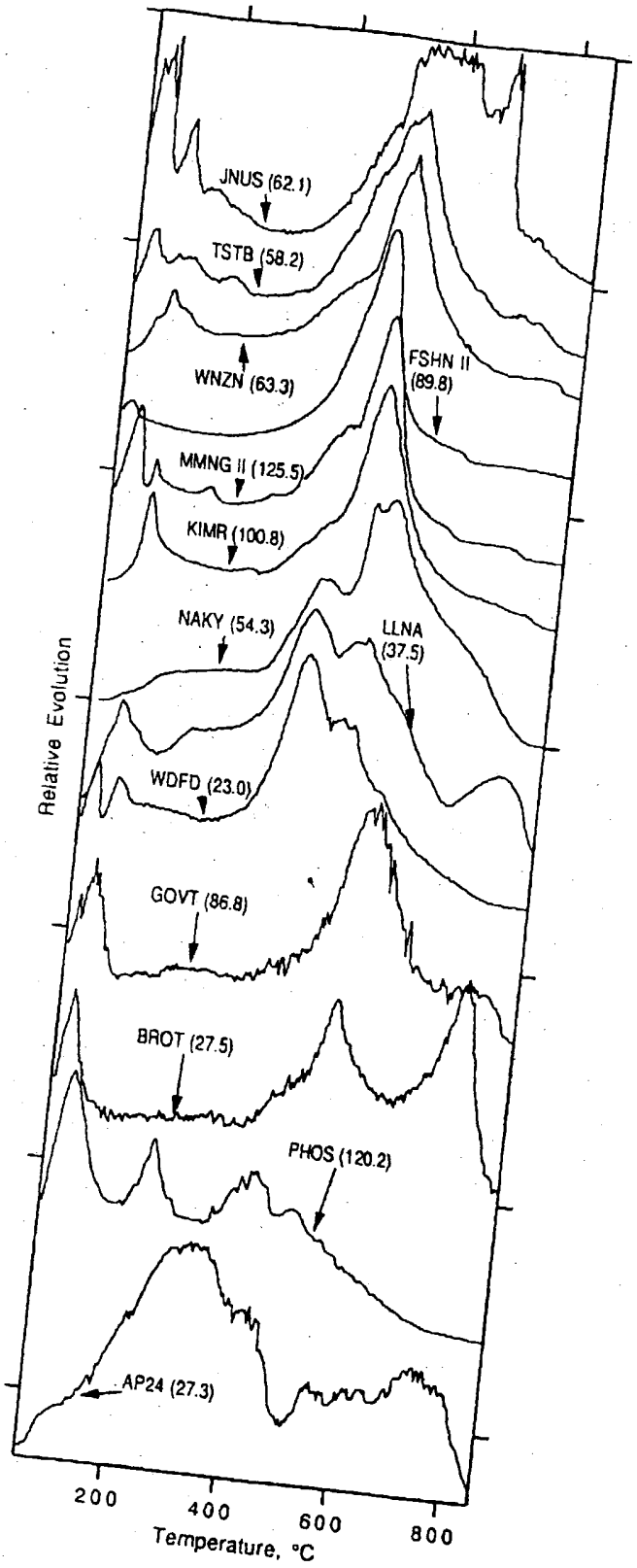
JNUS (62.1)
TSTB (58.2)
WNZN (63.3)
FSHN II (89.8)
MMNG II (125.5)
KIMR (100.8)
NAKY (54.3)
LLNA (37.5)
WDFD (23.0)
GOVT (86.8)
BROT (27.5)
PHOS (120.2)
AP24 (27.3)
Relative Evolution
200
400
600
800
Temperature, °C

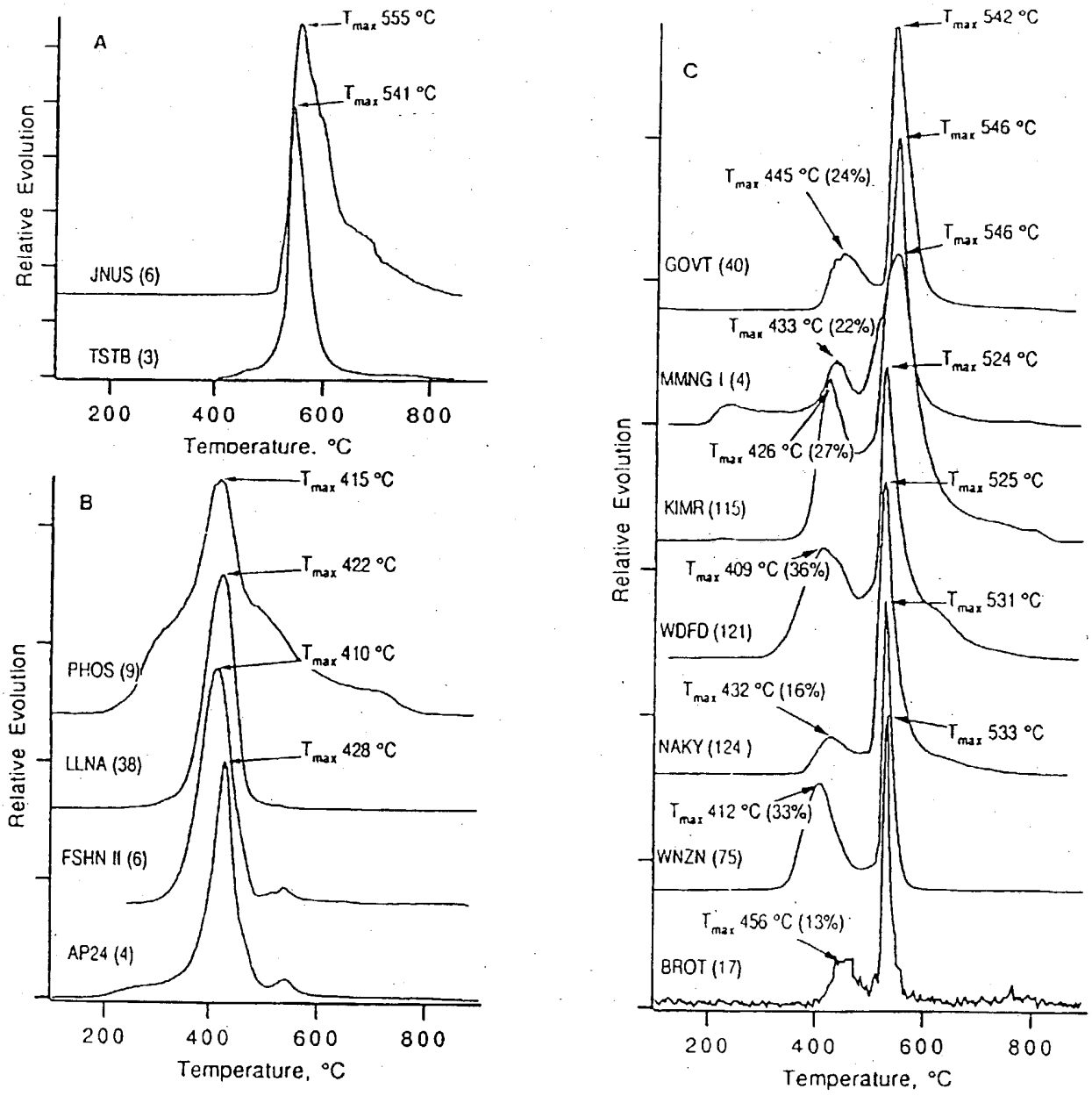
A
T_{max} 555 °C
T_{max} 541 °C
JNUS (6)
TSTB (3)
Relative Evolution
200
400
600
800
Temperature, °C
B
T_{max} 415 °C
T_{max} 422 °C
T_{max} 410 °C
T_{max} 428 °C
PHOS (9)
LLNA (38)
FSHN II (6)
AP24 (4)
Relative Evolution
200
400
600
800
Temperature, °C
C
T_{max} 542 °C
T_{max} 546 °C
T_{max} 445 °C (24%)
T_{max} 546 °C
GOVT (40)
T_{max} 433 °C (22%)
MMNG I (4)
T_{max} 524 °C
T_{max} 426 °C (27%)
KIMR (115)
T_{max} 525 °C
T_{max} 409 °C (36%)
WDFD (121)
T_{max} 531 °C
T_{max} 432 °C (16%)
NAKY (124)
T_{max} 533 °C
T_{max} 412 °C (33%)
WNZN (75)
T_{max} 456 °C (13%)
BROT (17)
Relative Evolution
200
400
600
800
Temperature, °C

Figure 9

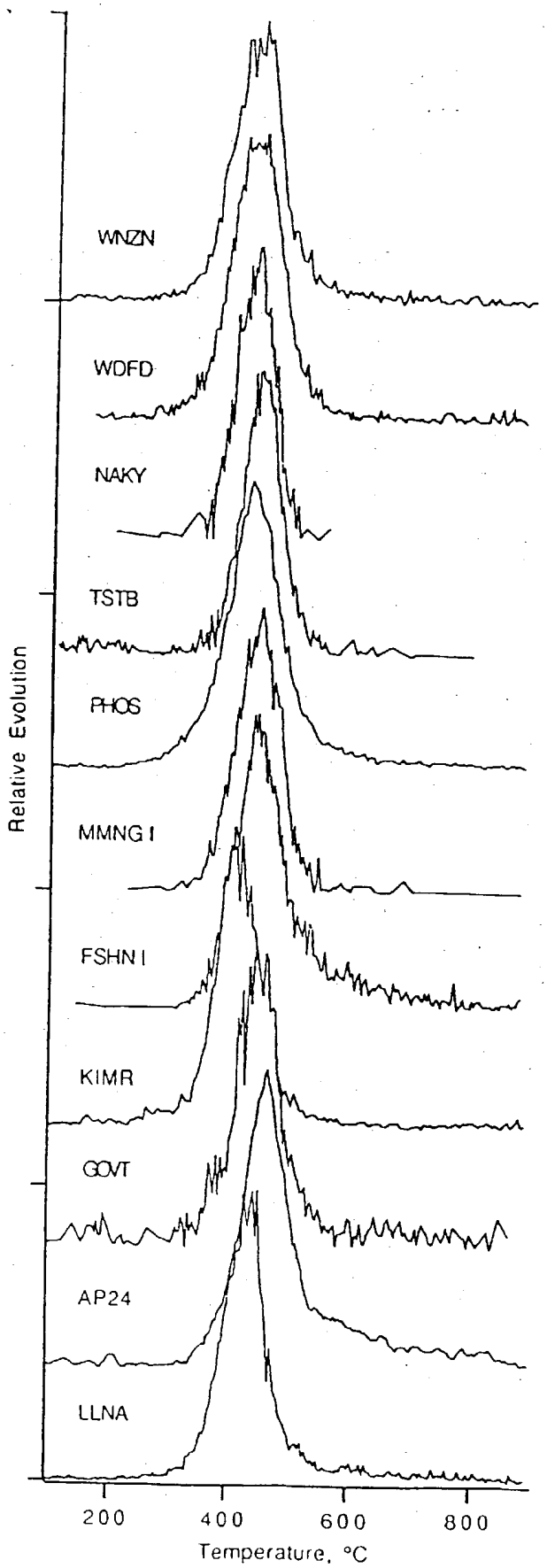
WNZN
WDFD
NAKY
TSTB
PHOS
MMNG I
FSHN I
KIMR
GOVT
AP24
LLNA
Relative Evolution
200
400
600
800
Temperature, °C

Figure 10

Figure 11

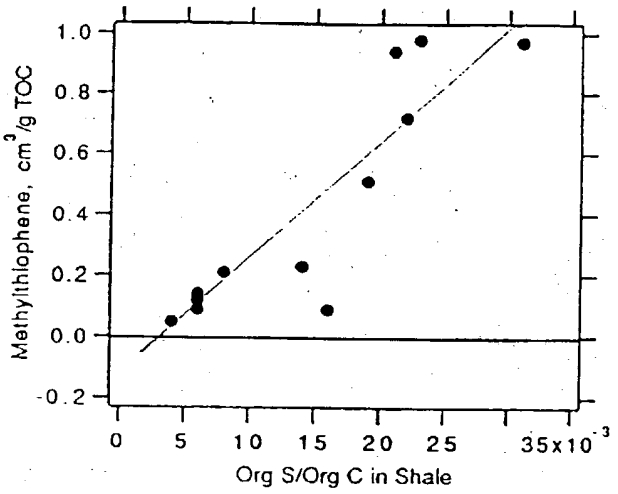
1.0
0.8
0.6
0.4
0.2
0.0
-0.2
Methylthiophene, cm³/g TOC
0
5
10
15
20
25
35x10⁻³
Org S/Org C in Shale

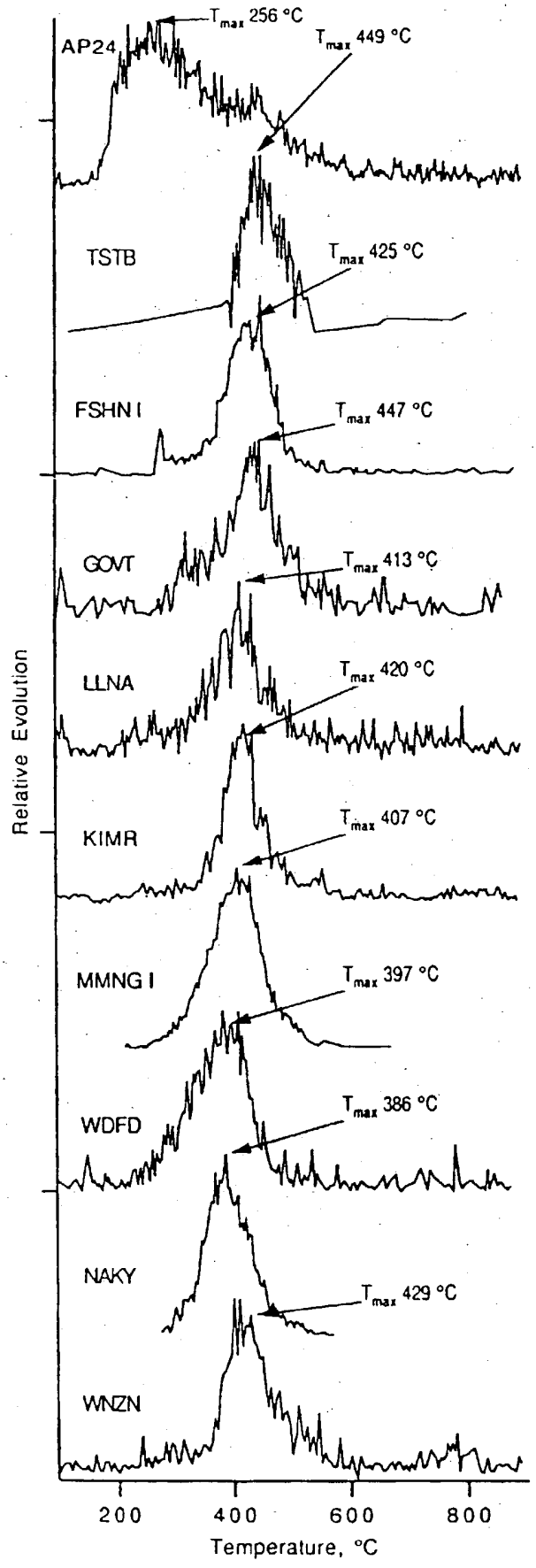
AP24
T_{max} 256 °C
T_{max} 449 °C
TSTB
T_{max} 425 °C
FSHN I
T_{max} 447 °C
GOVT
T_{max} 413 °C
LLNA
T_{max} 420 °C
KIMR
T_{max} 407 °C
MMNG I
T_{max} 397 °C
WDFD
T_{max} 386 °C
NAKY
T_{max} 429 °C
WNZN
Relative Evolution
200
400
600
800
Temperature, °C